Ediacaran cap dolomite of Shennongjia, Northern Yangtze Craton, South China

Hongwei Kuang[a], Yongqing Liu[a], Nan Peng[a], Thomas M. Vandyk[b], Daniel Paul Le Heron[c], Zhicai Zhu[a], Huaqing Bai[d], Yuchong Wang[a], Zhixian Wang[e], Quan Zhong[e], Jinxin Chen[e],Huiliang Yu[e], Xiaoshuai Chen[a], Changgui Song[f], Kening Qi[g],*

[a] *Geology Institute, Chinese Academy of Geological Sciences (CAGS), No. 26 Baiwanzhuang Road, Xicheng District, Beijing, 100037, China*

[b] *Royal Holloway University of London, Egham, Surrey, TW20 0EX, United Kingdom*

[c] *Department of Geology, University of Vienna, Althanstrasse 14, A-1090 Vienna, Austria*

[d] *Chinese Academy of Geological Sciences (CAGS), No. 26 Baiwanzhuang Road, Xicheng District, Beijing, 100037, China*

[e] *Shennongjia National Park Administration, No.36, Chulin Road, Shennongjia, 442421, China*

[f] *China University of Mining and Technology, Beijing, Ding No.11 Xueyuan Road,Haidian District, Beijing, 100083, China*

[g] *Hefei University of Technology, Hefei, No.193, Tunxi road, Baohe District, 230009, China*

Corresponding author: Yongqing Liu

E-mail address: liuyongqing@cags.ac.cn

Abstract: Ediacaran cap dolomites are strong evidence for the glaciation during the Neoproterozoic. Stratigraphic-sedimentological studies combined with $\delta^{13}C$ and $\delta^{18}O$ isotope analyses are used for defining the processes of post-glacier environmental changes and sea-level rise caused by glacier melting and the reconstruction of the depositional environments for the Doushantuo cap dolomites in Shennongjia, northern Yangtze Craton (YC). Like many other cap dolomites in the YC and worldwide, those in Shennongjia exhibit strongly negative $\delta^{13}C_{carb}$ excursions, ranging from -7.3 to -2.5 ‰ (averagely from -5.4 to -4.1 ‰). A laminated clast-free calcareous siltstone commonly occurs between the cap dolomite and the underlying diamictites, indicating a low-energy, shallow-water depositional environment, wherein alkaline conditions developed before the deposition of the cap dolomite. The most prominent features of the cap dolomites in Shennongjia are the very small thickness and monotonous sedimentary structures. The maximum thickness of the cap dolomites from the six sections in Shennongjia is 1.8 m, and the thinnest cap dolomite is 0.4 m with simple laminations. Sedimentary structures such as low-angle cross-bedding, giant wave ripples, sheet-crack cement, and tepee breccias are rare in Shennongjia except in the area near the

Three Gorges. These evidences, therefore, point to the deposition of the Shennongjia cap dolomite in restricted shallow-water tidal environments.

The space-time distribution of sedimentary facies in Shennongjia and the southeastern areas to Shennongjia indicate that the Ediacaran cap dolomite was formed on a ramp. Accordingly, we propose a sedimentary facies model for the formation of the cap dolomite, covering the inner and middle ramp facies. This model explains the thickness variations and distributions of the cap dolomites at both the local and regional scale, including their sedimentary structures, compositions, and barite occurrences. The model successfully illustrates why the cap dolomites in the Shennongjia area share a unique set of sedimentary features. Finally, the cap dolomite is interpreted as a diachronous deposit (bottom to top), tracking glacioeustatic flooding and recording ocean-wide changes over the time following deglaciation, and a correlation and cause of negative $\delta^{13}C_{carb}$ excursions in cap dolomites worldwide, particularly in those in the Yangtze Carton, are further discussed.

Keywords: Ediacaran; Cap dolomite; Sedimentology; Paleogeography; Shennongjia; Yangtze Craton, South China

1. Introduction

Rapid warming and sea-level rise following the late Cryogenian snowball Earth events (635 Ma) led to the global deposition of cap dolomites (Kaufman et al., 1997; Hoffman et al., 1998; Christie-Blick et al., 1999; James et al., 2001; Kennedy et al., 2001a, 2001b; Hoffman and Schrag, 2002; Jiang et al., 2003a; Ridgwell et al., 2003; Walter et al., 2003; Porter et al., 2004; Xiao et al., 2004; Zhou et al., 2004). The widely distributed cap dolomites in the Yangtze Craton (YC), South China, are considered to have been deposited following the Marinoan glaciation and have been associated with the global transgression during the glacioeustatic flooding of continental margins and inland areas as ice sheets receded. Hoffman et al. (2011) suggested that cap dolomites worldwide primarily consist of fine dolomites, peloids, tubestone stromatolites, tepee breccias, and barite (crystal fans), with a thickness varying

from a few meters to hundreds of meters. Distinctive sedimentary structures such as low-angle cross-laminae, giant wave ripples, and sheet-crack cements are common in these cap dolomites and are considered to result from a series of petrological, sedimentological, biological, mineralogical, and geochemical changes caused by the abrupt global warming postdated global glaciation. Over the past decades, numerous studies have focused on the cap dolomite within the YC (Jiang et al., 2003a, 2003b, 2006a, 2011; Zhu et al., 2007a, 2007b, 2013; Zhou et al., 2010, Liu et al., 2014a). However, important questions related to the sedimentary facies interpretation and the formation model for the cap dolomites remain controversial. One of the popular and traditional views is that the cap dolomites represent a spatial-temporal transition of sedimentary facies from a shelf to a slope environment, and then to a basin (Hoffman et al., 1998; Hoffman and Schrag, 2002; Jiang et a1, 2011).

However, the particular sedimentary structures mentioned above are very rare in the cap dolomites in the Shennongjia area of the northern YC, South China. In contrast, the cap dolomites in this area display very simple and monotonous sedimentary structures in the form of laminations. It is also important to note that the cap dolomites in Shennongjia are very thin, with a minimum thickness of 0.4 m and the maximum thickness of 1.8 m in the six sections shown in Figure 1. In addition, the cap dolomites in Shennongjia display either a sharp contact with or a cyclic dolomite-siltstone transition from the underlying glacial deposits. Moreover, laminated clast-free calcareous siltstones commonly occur between the cap dolomite and the underlying diamictites, indicating a shallow-water, low-energy depositional environment, in which alkaline conditions developed prior to the deposition of the cap dolomite. The topmost glacial deposits, the cap dolomite, and the overlying sediments are occasionally rich in algae and organic matter. These features provide important information concerning the depositional mechanism for the cap dolomite. From this perspective, the sedimentary structures described in previous studies that indicate deep-water deposition of the cap dolomite may perhaps have other interpretations, and further discussion is needed. In particular, more detailed sedimentological studies concerning the processes associated with post-glacier environmental changes and sea-level rise in the aftermath of snowball Earth are

required.

Furthermore, many studies on the carbon isotope $^{13}C_{carb}$ in dolomite have claimed that significant $^{13}C_{carb}$ gradients or $^{13}C_{carb}$ spatial variations exist in the cap dolomites of different sedimentary facies, from the inner shelf, through the continental slope, to the basin of the YC (Fig.2, Zhou et a1., 2004; Shen et a1., 2005; Jiang et a1., 2007, 2011; Peng et a1., 2016). However, compared with the researches focused on the Doushantuo Formation in other areas in the YC (Li and Leng, 1987; Deng et al., 2015; Ye et al., 2015; Guan et al., 2016; Wang et al., 2017), studies concerning the Doushantuo Formation and the cap dolomite in the Shennongjia area are few. Among these studies, Peng et al. (2011) and Yang et al. (2019a) published new data concerning barite and Mo isotopes in the cap dolomite in Shennongjia, and $^{13}C_{carb}$ spatial variations were briefly described by Wang et al. (2017). Considering the several differences between the cap dolomites in Shennongjia and elsewhere in the YC or in other locations worldwide, it is worthy to find out what is the $^{13}C_{carb}$ gradient or $^{13}C_{carb}$ spatial variation in the very thin cap dolomite in Shennongjia. In addition, the paleogeography of the cap dolomite at the beginning of the Ediacaran in YC is poorly studied and is debated, and previous reconstructions of the paleogeography of the cap dolomite of the Doushantuo Formation are confusing.

The research presented in this paper represents an integrated study of the Ediacaran cap dolomite in the Shennongjia area, based mainly on the spatial distribution, sedimentology, and carbon-oxygen geochemical data from six new sections (Fig. 1), as well as a reappraisal of three sections identified by Wang et al. (2017). In particular, sedimentological features and the evolution of the sedimentary environment during the icehouse–greenhouse transition and post-glacier period are described in more detail. Finally, a model is proposed for the precipitation of the cap dolomite and the Early Ediacaran paleogeography in Shennongjia. These data facilitate a refined understanding of the Ediacaran cap dolomite in the Shennongjia area and could be used to inform reconstructions of the environmental, geochemical, and paleogeographic conditions that characterized the unusual and abrupt warming which shook the Earth free from its deep-freeze condition.

2. Geological setting

The YC was amalgamated with the Cathaysia Block prior to the Cryogenian (ca. 0.9–0.8 Ga) (Shu et al., 2011; Wang et al., 2013; Zhang et al., 2013a; Zhang et al., 2013b; Geng, 2015; Zhao, 2015; Yao et al., 2015, 2016) and is bounded by the Qinling-Dabie orogenic belt in the north and the Longmenshan fault zone in the west (Zhao and Cawood, 2012), where Mesoproterozoic and Neoproterozoic strata are widely exposed. The Shennongjia area, located in the northern margin of the YC (Fig. 1), is a structural dome covering an area of more than ~l, 800 km^2, comprising the Mesoproterozoic Shennongjia Group in the core and the surrounding late Neoproterozoic to Phanerozoic strata. The Archean–Paleoproterozoic basement of the YC, consisting of the Kongling high-grade metamorphic rocks (i.e., Archean TTG (Trondhjemite，Tonalite，and Granodiorite) and Paleoproterozoic metasedimentary rocks) (Shu et al., 2011; Wang et al., 2013; Geng, 2015) located in the southeast of the study area, is unconformably overlain by the Mesoproterozoic Shennongjia Group and the Neoproterozoic–Paleozoic deposits. However, the contact surface between the Kongling basement rocks and the Shennongjia Group is not exposed (Kuang et al., 2019).

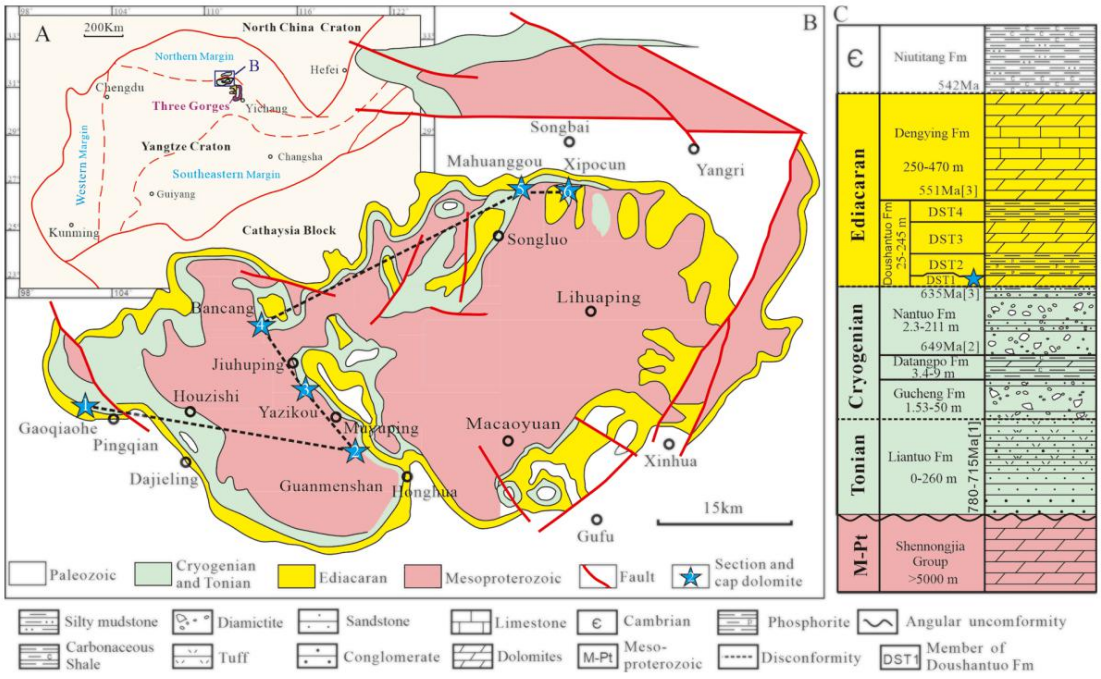

Fig. 1 Geological map showing the stratigraphy of the Yangtze Craton and the distribution of the Ediacaran cap dolomite (blue stars) in the Shennongjia area. (A) Geographic position of the

Yangtze Craton in South China and location of the study area (Shennongjia); (B) Distribution of the different stratigraphic units in the study area and location of the six cap dolomite sections in Shennongjia: 1 – Gaoqiaohe section; 2 – Guanmenshan section; 3 – Yazikou section; 4 – Bancang section; 5 – Mahuanggou section; and 6 – Xipocun section; (C) Neoproterozoic stratigraphic column of the Shennongjia area. Chronological data marked [1] are from Song et al. (2017), [2] are from Zhou et al. (2019), and [3] from Condon et al. (2005). (For interpretation of the references to color in this figure legend, the reader is referred to

the web version of this article.)

The Mesoproterozoic Shennongjia Group is ~10,000 m thick and mainly composed of bathyal and shallow-sea sedimentary rocks. It is subdivided into three subgroups and occasionally intruded by intermediate–basic volcanic rocks or basic sills and dykes, which are considered to represent a record of the breakup of the Columbia Supercontinent (Kuang et al., 2019). On the northern margin of the YC, the Neoproterozoic strata generally include the late Tonian Liantuo Formation, the early Cryogenian Gucheng/Tiesiao/Dongshanfeng formations (Sturtian Glaciation), the middle Cryogenian Datangpo Formation (interglaciation), the late Cryogenian Nantuo Formation (Marinoan Glaciation), and the Ediacaran Doushantuo and Dengying formations, in ascending order (Lu et al., 1985, 1987; Guan et al., 2016) (Fig. 1C). The Early Neoproterozoic Tonian and Cryogenian strata record the breakup of the Rodinia Supercontinent (Shu et al., 2011; Yang et al., 2019b). These are widely distributed in Shennongjia and other areas of the YC and are characterized by significant variations in either stratigraphy and lithological associations or sedimentological features (Zhang and Chu, 2007; Yin and Gao, 2013; Lan et al., 2015; Zhou, 2016; Zhu et al., 2016; Song et al., 2017; Zhou et al., 2019a).

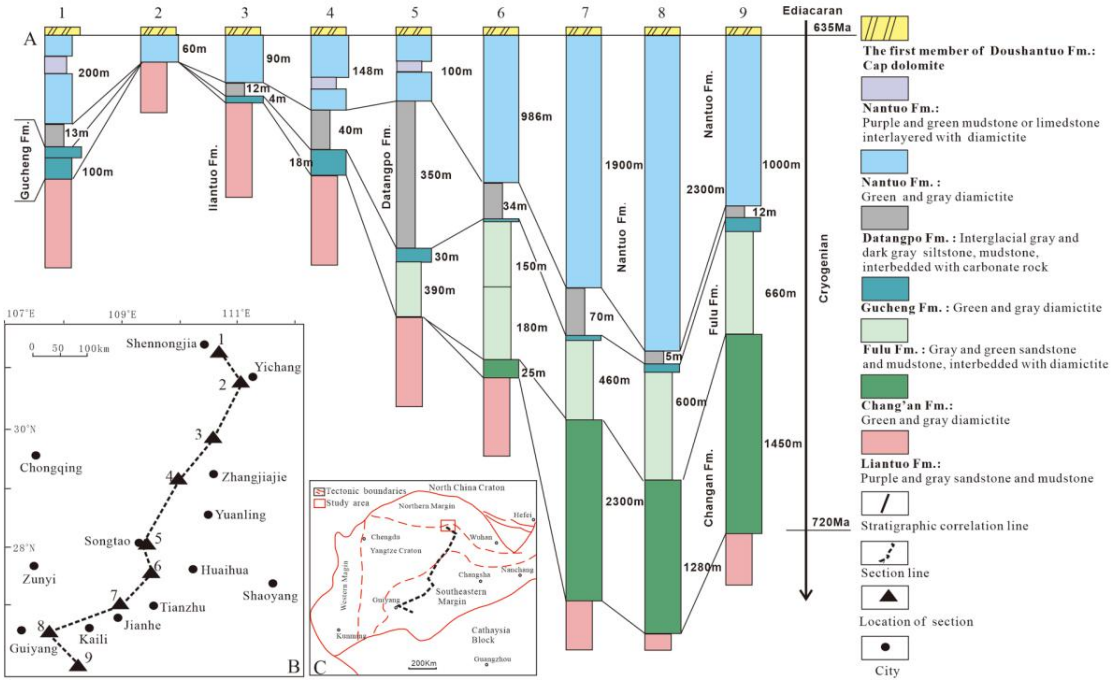

Fig. 2 Correlations of the Cryogenian strata in the Yangtze Craton, South China. (A) Stratigraphic correlation framework of Neoproterozoic Cryogenian strata in the Yangtze Craton. Cryogenian consists of the Chang'an, Fulu, Gucheng and/or Tiesiao/ Dongshanfeng, and Nantuo formations. The Cryogenian strata are underlain by the Tonian Liantuo Formation and overlain by the Ediacaran Doushantuo Formation. The thickness is mainly modified from Zhu et al. (2016). The correlation line (black dashed line) is marked in (B). The numbers in (A) and (B) refer to the locations of the sections: 1 – Shennongjia area in Hubei province; 2 – Three Gorges; 3 – Yangjiaping in the northwest of Hunan Province; 4 – Longbizui in the west of Hunan Province; 5 – Songtao in the northeast of Guizhou Province; 6 – Hongjiang in the northeast of Hunan Province; 7 – Qianyang in the northwest of Hunan Province; 8 – Lijiapo in Congjiang, Guizhou Province; 9 – Jiangshixian in Sanjiang, Guizhou Province. (C) Location of the stratigraphically correlated line and position of the research area in the Yangtze Craton.

The Ediacaran Doushantuo and Dengying formations span from the north to the southeast of the YC. The Doushantuo Formation hosts the cap dolomite and bears the Weng'an biota, which is considered to comprise the earliest animal embryo fossils known to date, or acritarch and algae fossils such as the Xilingxia biota and Miaohe biota, which are older than the Ediacaran fossils (Yin et al., 2007; Yin et al., 2009a, 2009b; Liu et al., 2014c; Xiao et al., 2014). This Formation commonly distinctively overlies the Cryogenian Nantuo Formation comprising of massive sandy and calcareous diamictites and dropstone-bearing laminated

mudstone/siltstone and locally overlies the Mesoproterozoic Shennongjia Group. The Doushantuo Formation is further subdivided into four lithological units, which are, in ascending order, the basal unit (first member of the Doushantuo Formation, DST1) composed of cap dolomite; second unit (DST2) dominated by siltstone interbedded with thin dolomite layers; third unit (DST3) consisting of thick ribbon dolomite and dark black siltstone; and fourth unit (DST4) at the top primarily comprising dolomite concretions. The cap dolomites mainly comprise fine dolomites of variable thicknesses across the YC. These dolomites exhibit either transitional or sharp contact with the underlying Cryogenian Nantuo Formation. The SHRIMP U-Pb mean ages of tuff layers from the bottom to top of the cap dolomite are 635.23 ± 0.57 Ma (Condon et al., 2005) and 634.57 ± 0.88 Ma (Zhou et al., 2019b), respectively, which bracket the timescale of deposition of the cap dolomite ($<10^6$ yr). Phosphorites commonly occur in the DST2 and/or DST4 units in the YC, including the areas to the north of Three Gorges (Zhang et al., 2013c; An et al., 2015) and in eastern Shennnongjia (Peng et al., 2011; Wang et al. 2017); however, phosphorites are rare in DST2 in western Shennongjia. The Dengying Formation overlies the Doushantuo Formation and hosts tuff dated 551 Ma at its base (Condon et al., 2005). This Formation comprises chiefly dolomites and is ~250–470 m thick (Li and Leng, 1987) (Fig. 1C). These dolomites contain terminal Ediacaran algae and trace fossils, and are conformably overlain by Lower Cambrian dark gray carbonaceous shales (Zhou et al. 2019a).

3. Materials and methods

Six cap dolomite sections were measured and logged on a centimeter-scale. These sections are located at Gaoqiaohe (31°28’0.7” N, 110°5’16.9” E), Guanmenshan (31°27’22.3” N, 110°23’54.3” E), Yazikou (31°30’54.1” N, 110°20’12.5” E), Bancang (31°34’32.7” N, 110°20’3.9” E), Mahuanggou (31°41’15.8” N, 110°35’38.1” E), and Xipocun (31°41’55.5” N, 110°39’19.1” E). The sections at Guanmenshan, Yazikou, and Bancang (sections 2–4) are equally spaced along a 17.5 km SE–NW line, located 20–30 km east of the Gaoqiaohe section (section 1; Fig. 1). Each section contains a cap dolomite with a similar thickness of 0.6–0.7 m,

205 which conformably overlies the diamictites of the Nantuo Formation. The Mahuanggou
206 section is located in the central part of Shennongjia, ~80 km east to the Yazikou section and
207 10 km west to the Xipocun section. The lithology and sedimentary structures were described
208 in detail in the field and facies were divided based on these descriptions.
209 More than 100 cap dolomite samples were collected to prepare thin sections, and more than
210 60 of these samples were used for carbon and oxygen isotope analyses (Supplementary Table
211 1). Microscopic textures and structures, mineralogical components, and micro-organisms
212 were studied under the microscope using the thin sections. Carbon and oxygen isotopes were
213 measured using a MAT 253 mass spectrometer, coupled to a Kiel IV carbonate device, at the
214 National Key Laboratory of the Nanjing Institute of Geology and Paleontology, Chinese
215 Academy of Sciences. The laboratory temperature was 22 ℃ ± 1 ℃ and humidity was 50 %
216 RH ±5%. The reference standard was GBW-04405. The relative standard deviation (1SD) of
217 the measurements ($\delta^{13}C$ and $\delta^{18}O$, VPDB) was less than 0.030‰ and 0.080 ‰, respectively.
218 In addition, geochemical tests were performed on the matrix remained after the pebble-sized
219 clasts were removed for 19 samples of the Nantuo diamictites. Samples were first rinsed with
220 distilled water and ground into a homogeneous powder (200 mesh); then, they were flushed
221 with He gas for 12 min in a vacuum chamber to remove any remaining air. An injection of
222 100 % phosphoric acid (H_3PO_4) at 72 ℃ into the reaction flask was, then, carried out for at
223 least 96 min to ensure that the reaction was completed. The resulting CO_2 was brought into
224 the mass spectrometer by the He, where the C and O isotopic ratios were measured. Results
225 were calibrated with respect to international standard samples (NBS-18 and NBS-19) in the
226 laboratory and reported in delta notation (δ), in parts per thousand (‰) relative to the VPDB
227 standard. The results of the C and O isotope analyses are listed in Supplementary Table 1.
228 Major (Ca and Mg) and trace (Mn, Sr, and Fe) element analyses of carbonates were
229 performed at the National Key Laboratory of the Guiyang Institute of Geology and
230 Paleontology, Chinese Academy of Sciences. Precision and reproducibility for all analyzed
231 elements were greater than 10 %, according to replicate measurements of laboratory calcite
232 and dolomite standards.

Trace and major elements were determined by a Bruker Aurora M90 inductively-coupled plasma mass spectrometry (ICP-MS). About 0.0500 grams of powdered sample were placed in a PTFE bomb, and 1 ml of HF and 1 ml of HNO_3 were added. The sealed bombs were then placed in an electric oven and heated to 185°C for about 36 hours. After cooling, the bombs were heated on a hot plate to evaporate to dryness. 500 ng of Rh was added as an internal standard, and then 2 ml of HNO_3 and 5 ml of water were added. The bomb was again sealed and placed in an electric oven at 135 °C for about 5 hours to dissolve the residue. After cooling, the final dilute factor is about 3000 for trace elements measurement by ICP-MS and major elements by ICP-OES (Agilent 720). The SiO_2 was measured by traditional method of gravimetric. The sensitivity of the instrument was adjusted to about 350 000 cps (counts per second) for 1 ng ml^{-1} ^{115}In and 150 000 cps for 1 ng ml^{-1} of ^{232}Th using the normal sensitivity mode. The accuracies of the ICP-MS analyses are estimated to be better than ±5-10 % (relative) for most elements.

4. Results

4.1 C and O isotopes

According to the diagenesis tests, most of the cap dolomite samples underwent poor post-depositional diagenetic alteration and, therefore, preserve information regarding the syn-sedimentary marine oxygen and carbon isotopes in the Ediacaran. Thus, only very little data affected by diagenesis were excluded when plotting the isotopic data (e.g., sample DJH1-03-7 from the Gaoqiaohe section; Supplementary Table 1). A comparison of the $\delta^{13}C$ values from the Nantuo Formation, the cap dolomite, and the DST2 unit revealed that the Mahuanggou section displays the lowest $\delta^{13}C$ value (<-10 ‰) in the Nantuo Formation and the Guanmenshan section displays the second lowest value, while the other four sections display similar values between -7 and -3 $‰_{VPDB}$. The Xipocun section displays the highest $\delta^{13}C$ value (between -2.9 and -4.6 $‰_{VPDB}$). For cap dolomite, all the $\delta^{13}C$ values are moderately negative, between -7.3 and -2.5 $‰_{VPDB}$, except the slightly higher values in the

Xipocun section (mostly > -4 ‰). Within the DST2 unit, the $\delta^{13}C$ values are in similar ranges as in the cap dolomites, occasionally showing a very small negative drift. Further details of the $\delta^{13}C$ values are described in the following section.

4.1.1 Diagenesis

Previous studies of Paleozoic and Proterozoic carbonates have shown that $\delta^{18}O$ is a very sensitive indicator of diagenetic processes; and trace element (Fe, Mn, and Sr) contents are also a powerful tool for assessing the degree of diagenesis (Banner and Hanson, 1990; Kaufman et al., 1991; Banner and Kaufman, 1994; Bartley et al., 2007). In this study, in addition to the carbon and oxygen isotopes measured in the six studied cap dolomite sections, the whole rock major and trace elements were measured in three sections (Gaoqiaohe, Guanmenshan, and Yazikou) to investigate the diagenetic processes in the Nantuo and Doushantuo formations. Cross-plots of the Mg/Ca ratio vs. $\delta^{18}O_{VPDB}$, Sr vs. $\delta^{18}O_{VPDB}$, Mn vs. $\delta^{18}O_{VPDB}$, Fe vs. $\delta^{18}O_{VPDB}$, Mn vs. Fe, and $\delta^{13}C_{VPDB}$ vs. $\delta^{18}O_{VPDB}$ are shown in Fig. 3.

In general, well-preserved, non-evaporitic Precambrian carbonates frequently record oxygen isotope compositions between approximately -6 and -9 ‰ (Frank amd Lyons, 2000; Kah, 2000). It is generally believed that oxygen isotopes lower than -10‰ may have been affected by diagenesis (Kaufman et al., 1993). The $\delta^{18}O$ results from this study reveal moderate to strong partitioning from approximately -14.2 to -3.3 ‰, primarily between -5 and -10 ‰, with lower $\delta^{18}O$ values (<-10 ‰) mostly occurring in the Gaoqiaohe section (Fig. 3). This indicates that most of the samples preserve the original sedimentary features, except some samples of the cap dolomite from the Gaoqiaohe section.

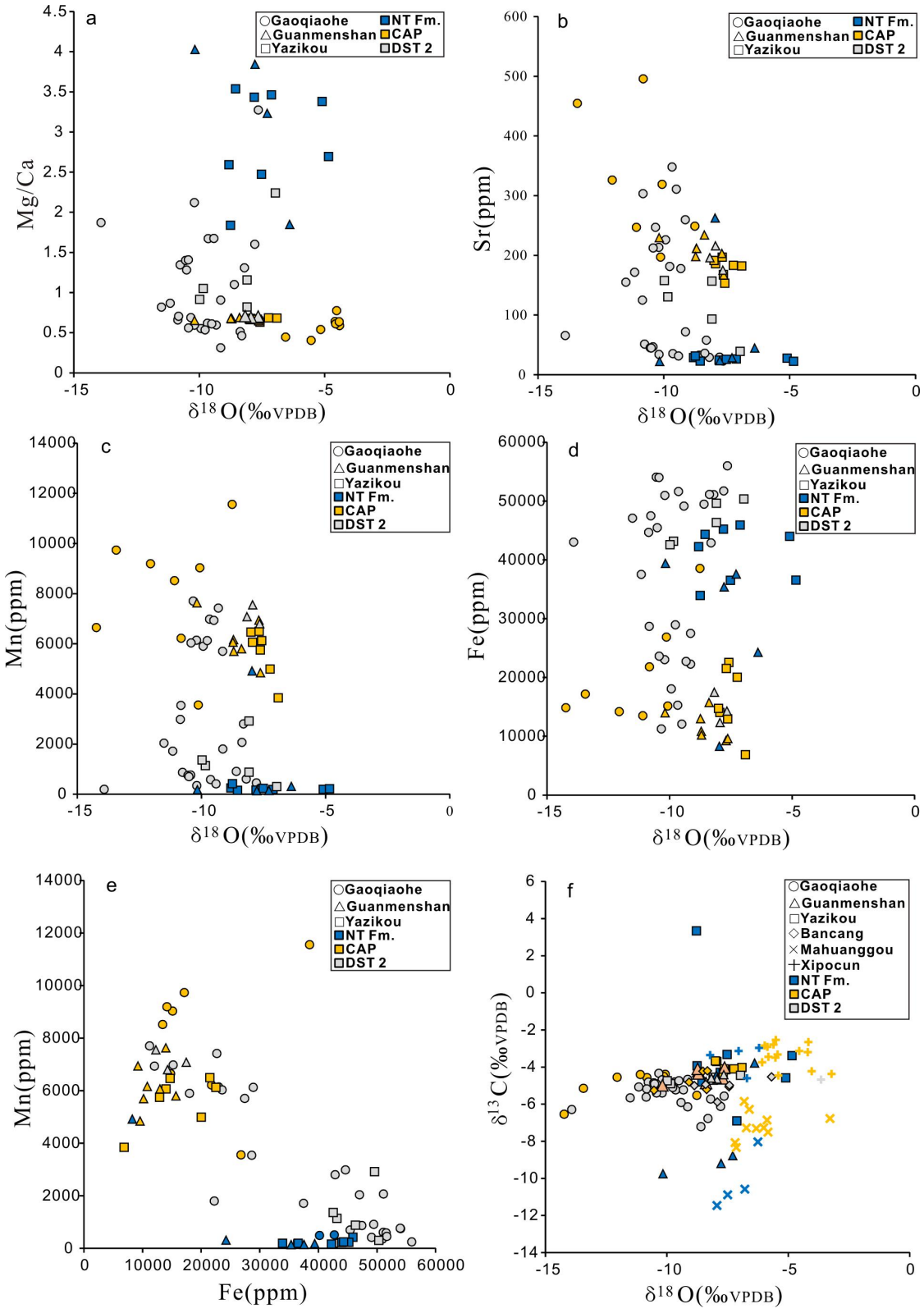

Fig. 3 Geochemical cross plots indicating the influence of diagenesis on the rock samples. Cross plots of (a–d) $\delta^{18}O$ vs. Mg/Ca, Sr, Mn, and Fe; (e) Fe vs. Mn; (f) $\delta^{18}O$ vs. $\delta^{13}C$. NT Fm. – Nantuo Formation; CAP – cap dolomite; DST2 – second member of the Doushantuo Formation.

The Mg/Ca ratio is typically >0.5 in dolomite and 0.1–0.5 in limestone (Bartley et al.,

2007). The Mg/Ca ratios in this study were in the range 0.3–4.5 (Fig. 3a), with lower ratios of 0.6–0.7 observed in the cap dolomite and higher ratios of 1.0–4.0 in the diamictite of the Nantuo Formation (primarily>3). In DST2, the Mg/Ca ratios display strong partitioning from -0.3 to 2.2 and suggest a limited post-diagenetic alteration in most of the dolomite samples.

It is difficult for Sr to enter into the dolomite lattice structure during dolomitization (Bartley et al., 2007). In the marine carbonate system, the Sr content changes only among different sedimentary rocks (Doe, 1973; Faure, 1977). The Sr contents in the Nantuo Formation are <35 ppm, primarily in the range of 0–20 ppm, whereas higher values from 150 to 500 ppm occur in the cap dolomites. In DST2, the Sr contents are mainly concentrated in the 150–250 ppm range and rise in a fluctuating manner (Fig. 3b). The Sr content displays a weak negative correlation with the $\delta^{18}O$ values.

An increase in the Mn content typically results from two situations. One is due to the carbonate deposition from manganese-rich reductive water (or microbial action), and the other owing to the alteration under burial conditions (Veizer et al., 1987; Bartley et al., 2007). The cross-plots reveal distinct disjointed and unrelated distribution relationships between $\delta^{18}O$ vs. Mn, $\delta^{18}O$ vs. Fe, and Fe vs. Mn (Fig. 3c-e). The Mn content is in the range of 86.8-11,500 ppm and Fe is in the range of 8,200-56,000 ppm. For most of the cap dolomite samples, the Mn content is >5,000 ppm and the Fe content is >10,000 ppm, with an uncorrelated relationship between Mn and Fe concentrations. The cap dolomites have high concentrations of Sr and Mn and intermediate concentration of Fe, which are uncorrelated with $\delta^{18}O$, indicating that the cap dolomites are almost unaffected by diagenesis.

The $\delta^{13}C_{VPDB}$ vs. $\delta^{18}O_{VPDB}$ diagrams also show a comparatively weak correlation (Fig. 3f). All of the above observations suggest that the obtained $\delta^{13}C$ and $\delta^{18}O$ values generally represent primary values from the time of deposition. Only occasional covariation is observed between $\delta^{13}C$ and $\delta^{18}O$, and the details of individual sections where this covariation occurs are described below. It has been argued that such a covariation can reflect depositional or diagenetic processes; however, only the $\delta^{18}O$ profile is likely to have changed if the latter occurred (Schobben et al., 2016).

4.2. Sedimentology and carbon isotope values ($\delta^{13}C$) of the cap dolomite sections

4.2.1 Gaoqiaohe section at Pingqian (section 1)

Section 1 is located on the western margin of the Shennongjia area (Fig. 1). This section is 8.3 m thick and displays a succession from the top of the Cryogenian Nantuo Formation, through the cap dolomite, to the lower Ediacaran Doushantuo Formation (DST2) (Fig. 4 and Supplementary Fig. 1). The Nantuo Formation is less than 2 m thick at the base of section 1. This Formation features medium and massive sandy conglomerates in the lower part (not shown in the stratigraphic column in Fig. 4), with pebbles of a few centimeters in size (Supplementary Fig. 1-1 A and B), typically subrounded–rounded, with a decreasing content upward. Laminated siltstone with dropstones of <1 cm in size is present in the middle of the Formation (Fig. 4, a and beds 1-2 in the stratigraphic column). On the top of the Formation, a calcareous clast-free silty mudstone with fine laminations or graded beds and small-scale ripples and truncations (Fig. 4, bed 2, b) is overlain by the cap dolomite with sharp contact (Fig. 4c and e), with a 1-2 cm-thick tuffaceous and calcareous mudstone with horizontal laminae occurring beneath the cap dolomite (Fig. 4c).

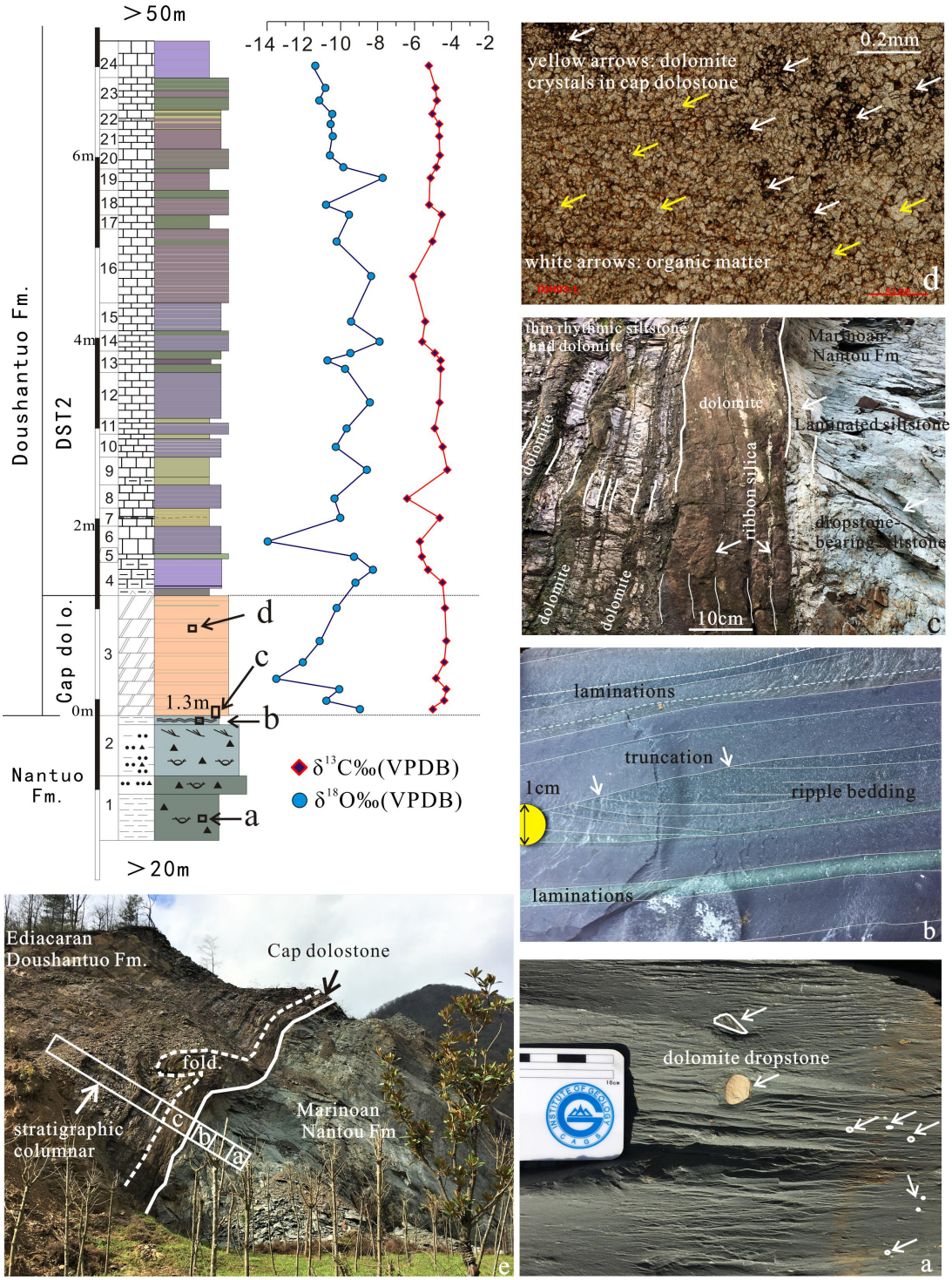

Fig. 4 Chemostratigraphy and sedimentology of the cap dolomite in the Gaoqiaohe section (section 1). In the measured section, the numbers indicate beds and the letters marked beside the lithological column indicate the locations of subfigures (a–e). (a) massive dropstone-bearing siltstone; (b) laminated and ripple-bearing clast-free siltstone with laminations and small-scale inclined bedding in the underlying diamictite; (c) rhythmically interbedded light gray siliceous muds and purple red–gray dolomite; (d) purple–red argillaceous dolomite with horizontal

bedding; (e) section from Marinoan Nantuo Formation to Ediacaran cap dolomite with the boundary between diamictite (right) and cap dolomite (left). Values of the C and O isotopes shown by the curves are given in Supplementary **Table 1. Color used in the lithological column reflects the surface color.**

The Doushantuo cap dolomite is 1.3 m thick (Fig. 4, bed 3, c) with primarily thin- and weakly-bedded to massive structures (Supplementary Fig. 1-1C). The cap dolomite is light pink to light gray (locally yellowish-brown) and occasionally contains discontinuous greenish-gray argillaceous ribbons (Fig. 4, bed 3, c). Bedding planes and sedimentary structures are rare within the cap dolomite. Microscopically, the cap dolomite is composed of homogenous and fine-grained crystalline dolomites with locally occurring black organic matter and pyrite or pseudo-framboid clusters (Fig. 4d and Supplementary Fig. 1-1 a-c). Above the cap dolomite, lies a set of, mainly, thin (centimeter-scale) rhythmically deposited light purple to red laminated calcareous siltstones and yellowish-gray dolomites belonging to the DST2 unit (Fig. 4, beds 4-24; Supplementary Fig. 1-1 D and E). Each rhythmic cycle is 10–20 cm-thick and are composed of mudstone in the lower part and dolomite in the upper part. The cyclic sequences become thicker upward, with the occurrence of horizontal and small-scale cross-bedding and graded beds. We note that the rhythmic dolomite is the same as the cap dolomite in terms of mineral composition, texture, and structure and differs only in thickness; however, the siltstones increase and gradually thicken upward, whereas the dolomite layers gradually decrease and become thinner.

Geochemically, the $\delta^{13}C$ values between the cap dolomite (bed 3: -6.5 to -4.4 ‰, n =8) and the overlying rhythmic cycles (beds 4–24: -7.2 to -4.3 ‰, n=27) are similar, with both displaying profiles with a jagged, rhythmic appearance showing both large and small deviations. There is generally no covariation between $\delta^{13}C$ and $\delta^{18}O$ in these units; however, positive correlations (r=0.85) are observed for the five samples, from DJH1-03-4 upward (Supplementary Table 1).

4.2.2 Guanmenshan section in Muyu town (section 2)

Section 2 is located in southwestern Shennongjia (section 2 in Fig. 1, Fig. 5). At the base of

the section, the Cryogenian Nantuo Formation (Fig. 5, bed 1) is a green to light gray massive diamictite (Fig. 5a and Supplementary Fig. 2A). Clasts inside the diamictite are rounded–angular grains of dolomite, sandstone, mudstone, and granite with small pebble or boulder sizes (Supplementary Fig. 2-2 a and b). Occasionally, decimeter-thick quartz arenite beds interrupt the diamictite, with the debris content and size of these layers decreasing upward. A 40 cm-thick layer of tuffaceous and calcareous mudstone with horizontal laminae also occurs between the top of the diamictite and the cap dolomite (Fig. 5, bed 2, lower b).

The cap dolomite is 66 cm-thick in this section and consists of white to brownish-yellow dolomite with horizontal bedding. The cap dolomite is separated from the laminated mudstone at the top of the Nantuo Formation by a distinct lithological interface; however, there is no evidence of erosion or discontinuity (Fig. 5, bed 3, middle b; Supplementary Fig. 2 B-D). Petrologically, the cap dolomite consists of homogenous fine-grained crystalline dolomite similar to that in the Gaoqiaohe section (Fig. 5, c, white arrows indicate dolomite crystals; Supplementary Fig. 2-2 c-f). Above the cap dolomite, the Formation consists of rhythmically deposited light purple–red laminated argillaceous siltstone and white–yellow argillaceous dolomite of few centimeters in thickness (Supplementary Fig. 2-1 E and F).

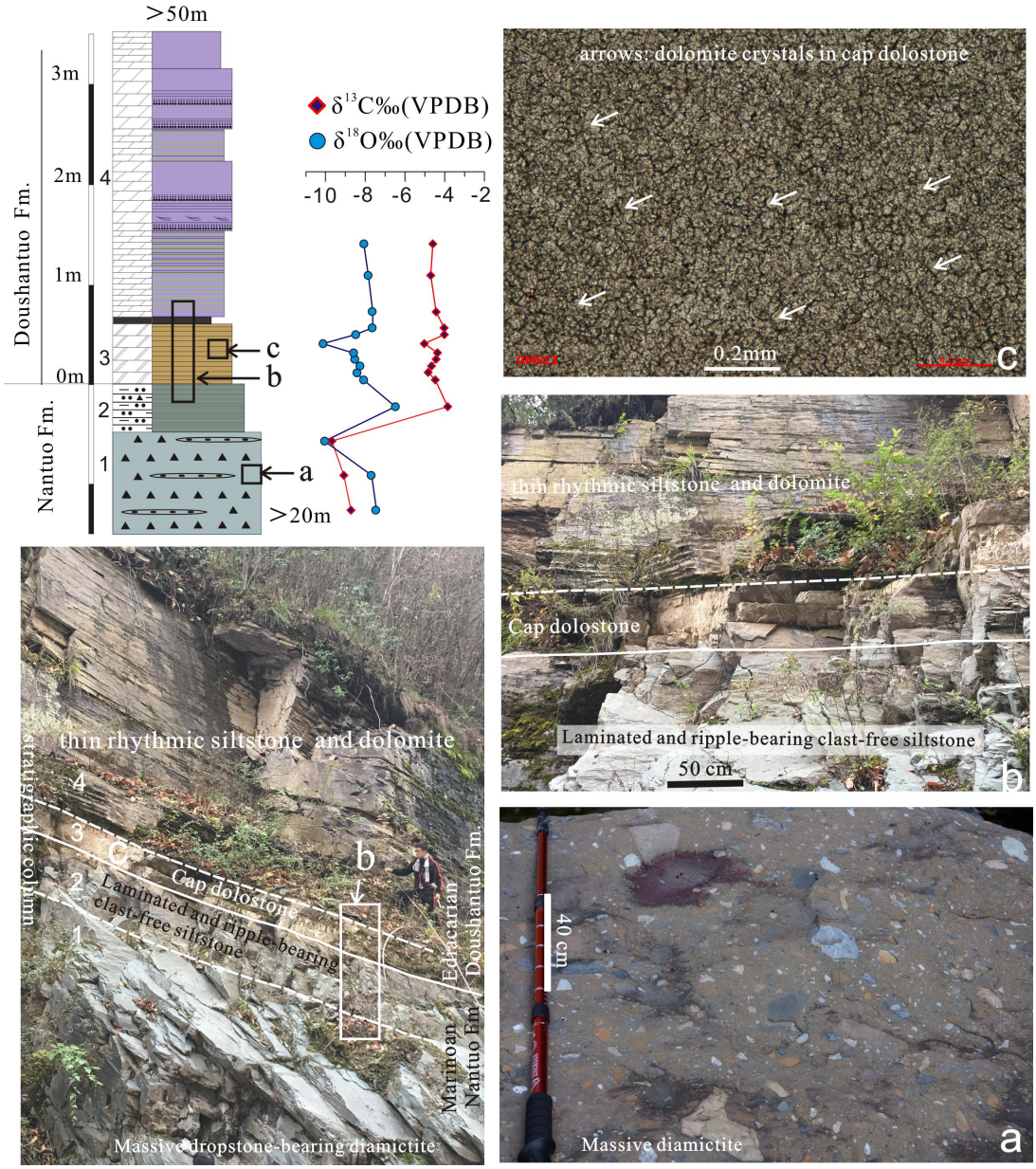

Fig. 5 Chemostratigraphy and sedimentology of the cap dolomite in the Guanmenshan section (section 2). In the measured section, the numbers indicate beds and the letters marked beside the lithological column indicate the locations of subfigures (a–c). (a) diamictites; (b) boundaries at the base and top of the cap dolomite, respectively; (c) microcrystalline dolomite fabric in the cap dolomite. See Fig. 4 for lithological and sedimentary structures legend. $\delta^{18}O$ and $\delta^{13}C$ values shown by the curves are given in Supplementary Table 1. Colors used in the lithological column reflect the surface colors.

Geochemically, $\delta^{13}C$ varies between -4.9 and -4.0 ‰ (n=7), and -4.6 and -4.4 ‰ (n=3) within the cap dolomite and in the overlying rhythmic beds, respectively (Fig. 5). The resulting Doushantuo Formation profile is slightly sinusoidal and there is no clear change in

391 $\delta^{13}C$ values between the upper and lower boundaries of the cap dolomite. The $\delta^{13}C$ values in
392 the uppermost 20 cm of the underlying diamictite are similar to those in the overlying cap
393 dolomite (-4.4 to -3.8 ‰, n=2), whereas the lowermost 30 cm contain significantly lighter
394 carbon isotopes (-9.8 to -8.8 ‰, n=3). Except these highly negative values at the base of the
395 section, there is a strong positive correlation between $\delta^{13}C$ and $\delta^{18}O$. In addition to the
396 microcrystalline dolomite fabric, the consistently negative $\delta^{13}C$ profile of the Doushantuo
397 Formation is a global diagnostic feature of the cap dolomite (Halverson et al., 2005).

398 4.2.3 Yazikou section at Jiuhuping (section 3)

399 The lower part of the Yazikou section (Fig. 1) is the top part of the Cryogenian Nantuo
400 Formation (Fig. 6, beds 11 and the underlying; Supplementary Fig. 3; Supplementary Fig.
401 3-1A) and consists of greenish to green–gray silty calcareous diamictite with abundant
402 randomly distributed clasts of <1 cm in diameter and composed of dropstone-like,
403 rounded-angular grains of dolomite, sandstone, mudstone, granite, etc. (Fig. 6 b and c;
404 Supplementary Fig. 3-1B). A light green calcareous mudstone of ~10 cm in thickness with
405 horizontal bedding is located beneath the cap dolomite and overlies the Nantuo Formation
406 with a distinct lithological boundary (Fig. 6, bed 11 and c; Supplementary Fig. 3-1C).

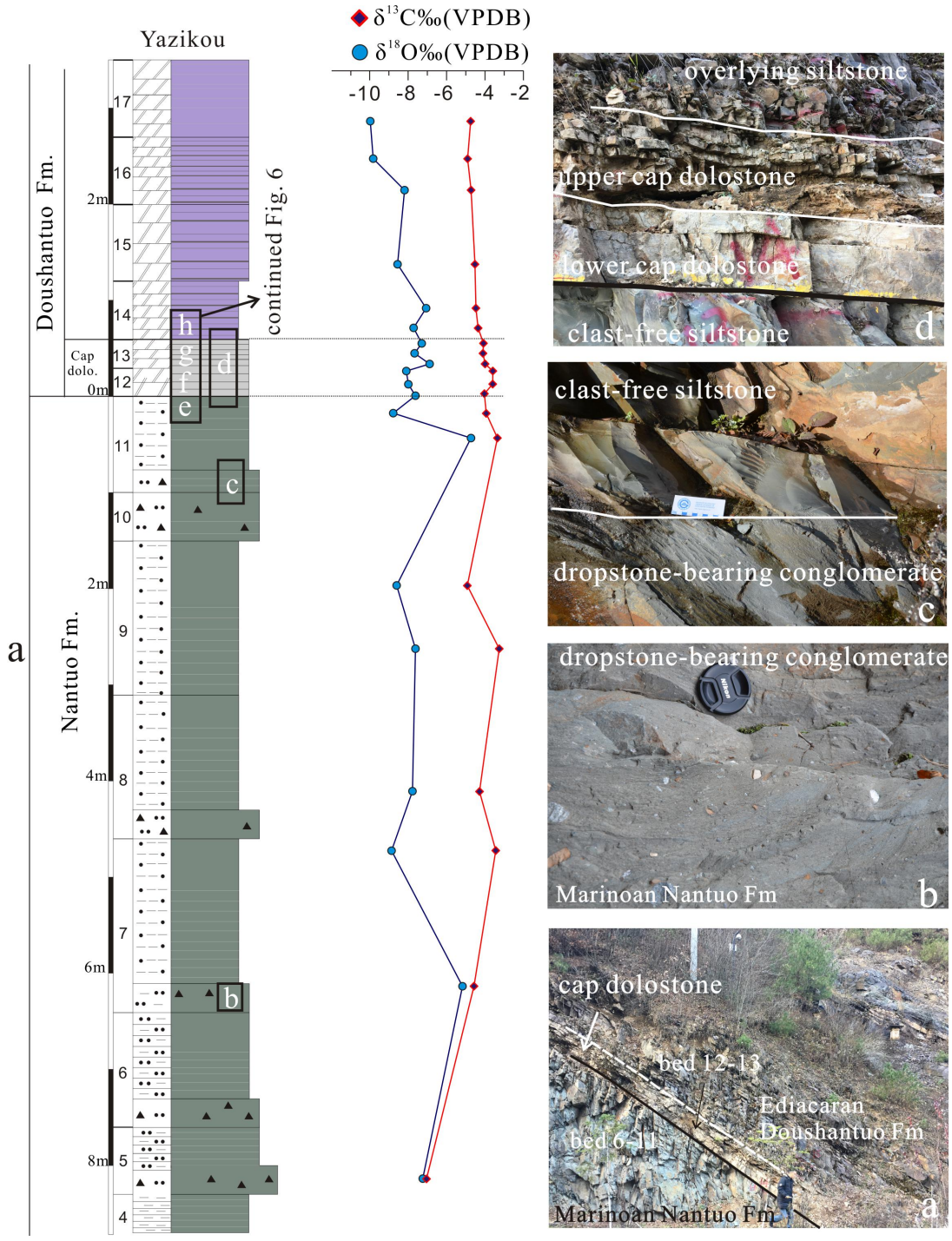

Fig. 6 Chemostratigraphy and sedimentology of the cap dolomite in the Yaizkou section (section 3). In the measured section, the numbers indicate beds and the letters marked beside the lithological column indicate the locations of subfigures (a–h). (a) sketch of the cap dolomite succession; (b) and (c) diamictites underlying cap dolomite in ascending order; (d) boundaries at the base and top of the cap dolomite, respectively. $\delta^{18}O$ and $\delta^{13}C$ values shown by the curves are given in Supplementary Table 1. See Fig. 4 for the lithological and sedimentary structures legend. Colors used in the lithological column reflect the surface colors. (e) light green calcareous

mudstone at the top of the Nantuo Formation displaying framboid pyrite; (f) cubic pyrite crystals have been replaced by dolomite in the lower cap dolomite, leaving a pseudo-pyrite morphology; (g) a small number of pyrite crystals in the upper cap dolomite; (h) organic matter and pyrite in the siltstone of the Doushantuo Formation.

The yellowish-white cap dolomite is 30 cm thick and overlies the light green calcareous mudstone in the upper part of the Nantuo Formation (Fig. 6, beds 12 and 13, d). Within the cap dolomite, the lower dolomites display horizontal bedding with layers of moderate thickness (Fig. 6, bed 12, d), while the upper dolomites are thinly-bedded and show no bedding (Fig. 6, bed 13, d). Above the cap dolomite, beds 14-17 (Fig.6, a) consist of rhythmically deposited thinly-bedded dolomites and siltstones of the Doushantuo Formation, with a gradual color transition from yellow to purple (Supplementary Fig. 3-1 D and E).

Petrologically, the cap dolomite consists of microcrystalline equigranular dolomite with the occurrence of pyrite (Supplementary Fig. 3-2 a-d). Pyrite is commonly observed in the top of the Nantuo Formation, in the cap dolomite, and in the overlying Doushantuo Formation, while framboid pyrite is concentrated in the green calcareous mudstone at the top of the Nantuo Formation and in the rhythmic thinly-bedded dolomites and siltstones of the Doushantuo Formation above cap dolomite (Fig. 6 continued, e and g). Notably, most of the cubic pyrites in the lower cap dolomite have been replaced by dolomite (Fig. 6 continued, f). The number of pyrite crystals in the upper cap dolomite is small (Fig. 6 continued, g) and increases upward in the overlying siltstone of the Doushantuo Formation. Organic matter is also abundant in the siltstone of the Doushantuo Formation (Fig. 6 continued, h).

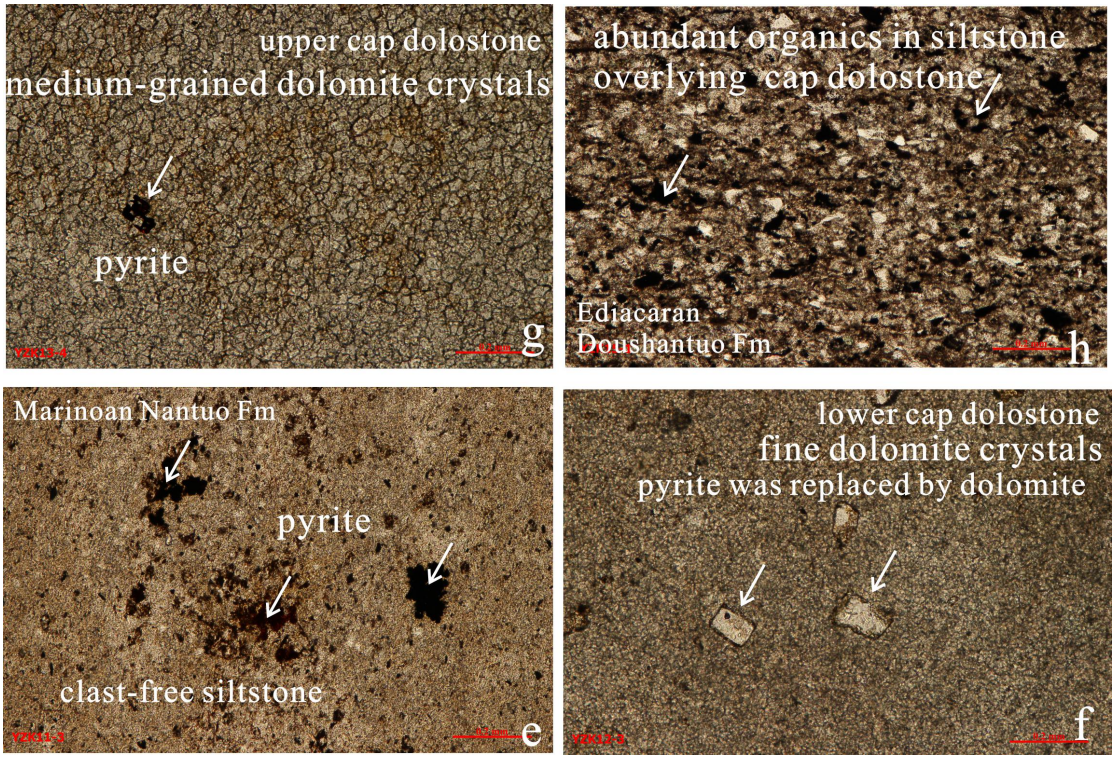

436

437 **Fig. 6 (continued)**

438 Geochemically, $\delta^{13}C$ values within the cap dolomite are between -4.1 and -3.7 ‰ (n=7) and
439 between -4.9 and -4.4 ‰ (n=5) in the overlying rhythmic beds (Supplementary Table 1).
440 There is no sharp change in $\delta^{13}C$ between the upper and lower units of the cap dolomite; thus,
441 a relatively straight profile of $\delta^{13}C$ through the cap dolomite and overlying rhythmic layers
442 with a slight decreasing upward trend is observed (Fig. 6). The $\delta^{13}C$ values in the uppermost
443 20 cm of the underlying light green calcareous mudstone at the top of the Nantuo Formation
444 also display a variation consistent with those observed in the overlying cap dolomite (-3.9 to
445 -3.4 ‰, n=2); $\delta^{13}C$ values in the lower 60 cm are much more variable (-6.9 to -3.3 ‰, n=6).

446 4.2.4 Bancang section at Liujiawuchang (section 4)

447 The top of the Nantuo Formation in the Bancang section (Fig. 1) consists of calcareous
448 mudstone characterized by no bedding, with scattered millimeter-sized dropstones (Fig. 7, BC
449 16; Supplementary Fig. 4 a and b). The lithology changes gradually upward (with no obvious
450 boundary) into a 70-cm thick weakly bedded light greenish-gray cap dolomite showing no
451 bedding (Supplementary Fig. 4-2). Petrologically, the cap dolomite is composed of
452 homogenous finely crystalline dolomite (Fig. 7, BC 22; Supplementary Fig. 4-1 g-i). Above

the cap dolomite lies a purplish-red, thinly-bedded rhythmic muddy dolomite (Fig. 7, BC 24). Many conspicuous filamentous and cloddy, dotted algae are present within the uppermost diamictites (Fig. 7, BC 16; Supplementary Fig. 4 c-f), the cap dolomite (Fig. 7, BC 22 Supplementary Fig. 4-1 j-l) and the dolomite of the overlying Doushantuo Formation (Fig. 7, BC 24). Framboid pyrite crystals are very abundant in the upper part of the cap dolomite (Fig. 7, BC 22).

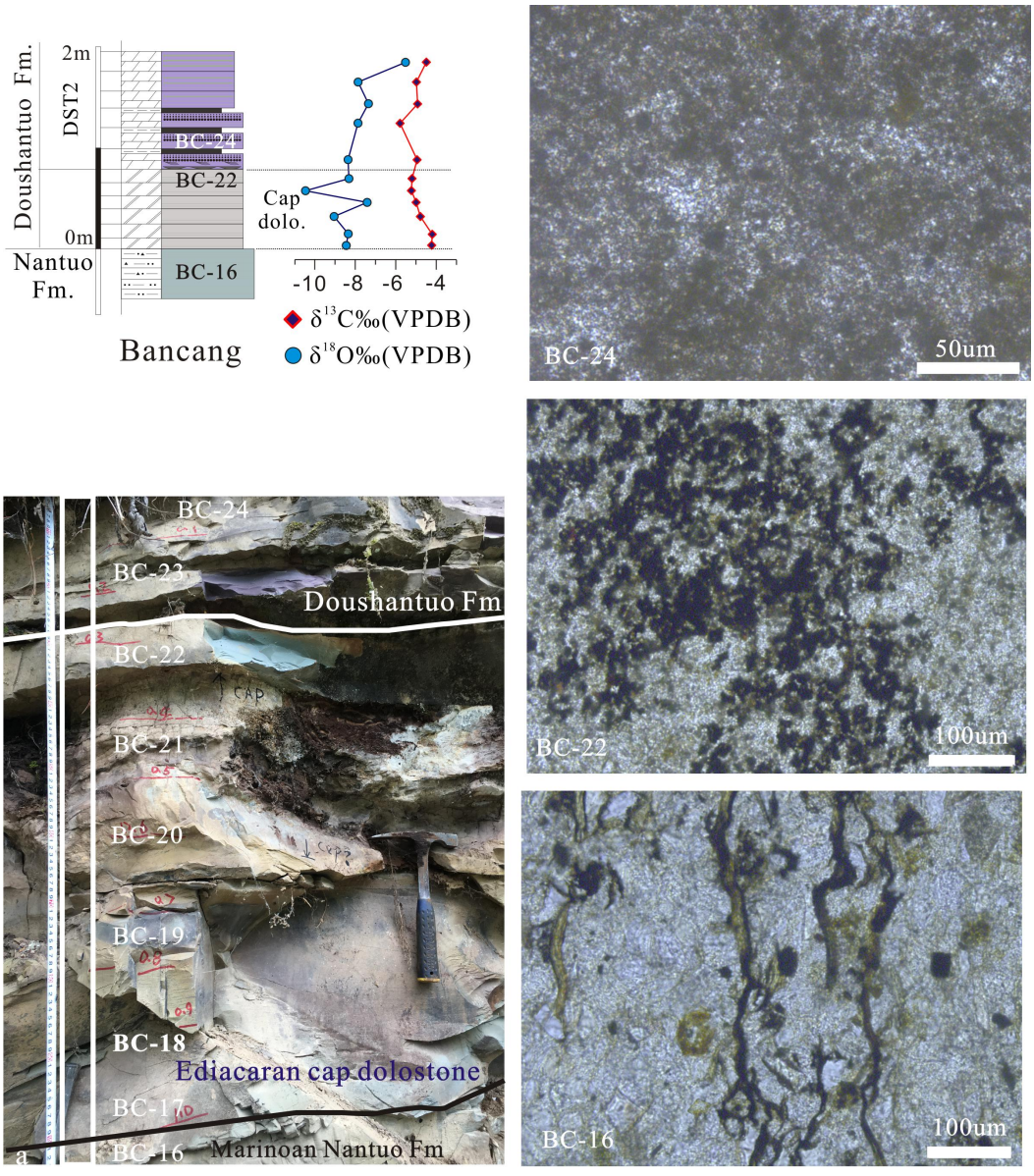

Fig. 7 Chemostratigraphy and sedimentology of the cap dolomite in the Bancang section (section 4). In the measured section, the numbers indicate beds. (a) cap dolomite and its top and basal boundaries; hammer for scale is 27.9 cm in length; (BC-16) filamentous and dotted algae in the underlying fine-grained diamictites of the Marinoan Nantuo Formation; (BC-22) filamentous and

dotted algae in dolomite; (BC-24) purple–red and gray–green rhythmic muddy dolomites in the overlying Doushantuo Formation. $\delta^{18}O$ and $\delta^{13}C$ values shown by the curves are given in Supplementary Table 1. See Fig. 4 for the lithological and sedimentary structures legend. Colors used in the lithological column reflect the surface colors.

Geochemically, the $\delta^{13}C$ values display a broad similarity in the cap dolomite (-5.3 to -4.2 ‰, n=6) and the overlying rhythmic beds (-5.9 to -4.5 ‰, n=4) (Fig. 7), despite a single negative outlier above the upper boundary of the cap dolomite. The negative $\delta^{13}C$ excursion is typical for the cap dolomite and no significant change in$\delta^{13}C$ value is observed between the interpreted cap dolomite and the overlying strata.

4.2.5 Mahuanggou section at Songluo village (section 5)

In section 5, the Nantuo Formation (bed 0 in Fig. 8) is composed of greenish–gray massive calcareous fine-grained diamictites with cm-scale pebbles, and the pebble content decreases upward (Supplementary Fig. 5A). A 10-cm thick yellowish–green tuffaceous, calcareous laminated mudstone (Fig. 8d) is directly overlain by the cap dolomite (bed 2) with a sharp conformable boundary (Supplementary Fig. 5 A-C). The cap dolomite is grayish yellow with a thickness of 40 cm and consists of finely microcrystalline homogenous and equigranular dolomite with horizontal bedding (Fig. 8e and Supplementary Fig. 5-1 a-d). Above the cap dolomite, beds 3-10 consist of cyclic depositions of grayish-green calcareous siltstone and yellow-gray dolomite with laminations (Fig. 8f). Each cycle is 25-30 cm-thick and is composed of a lower siltstone and an upper dolomite layer (Supplementary Fig. 5D). Importantly, the dolomites in these cyclic deposits are characterized by the same composition and sedimentary structures. These deposits are overlain by a sandstone turbidite sequence, indicating a deepening trend (Fig. 8, bed 11 and the overlying bed).

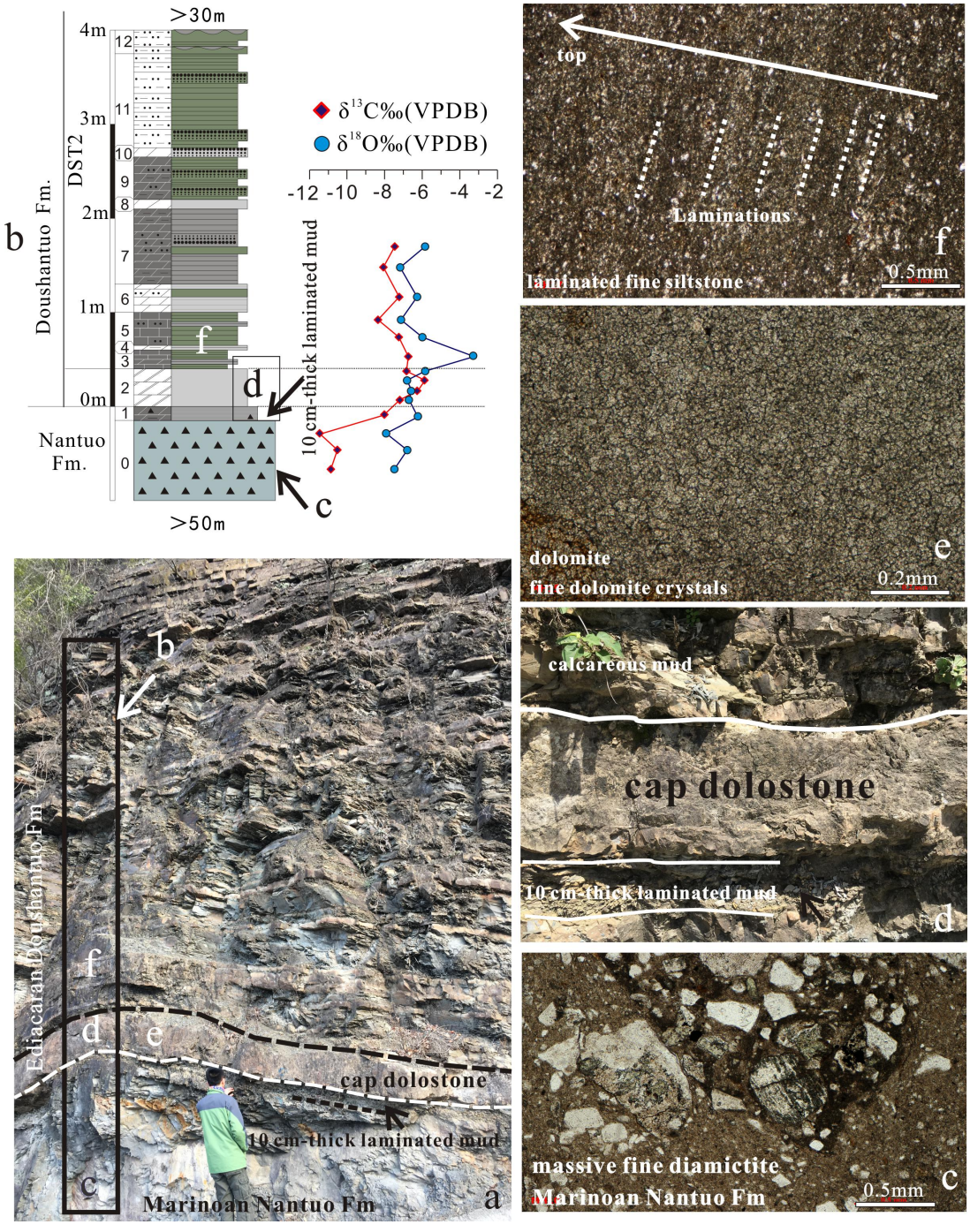

487

488 **Fig. 8 Chemostratigraphy and sedimentology of the cap dolomite in the Mahuanggou section**
489 **(section 5). In the measured section, the numbers indicate beds and the letters marked beside the**
490 **lithological column indicate the locations of subfigures (b–f). (a) cap dolomite and its top and**
491 **basal boundaries; human for scale in the right corner is 174 cm tall; (b) lithological column of**
492 **Mahuanggou section; (c) diamictite underlying the cap dolomite; (d) tuffaceous dolomite**
493 **interbedded between the diamictite of the Nantuo Formation and the cap dolomite of the**
494 **Doushantuo Formation; (e) microcrystalline dolomite in the cap dolomite; (f) laminated siltstone**

overlying cap dolomite. $\delta^{18}O$ and $\delta^{13}C$ values shown by the curves are given in Supplementary Table 1. See Fig. 4 for the lithological and sedimentary structures legend. Colors used in the lithological column reflect the surface colors.

Geochemically, the negative $\delta^{13}C$ values in the Nantuo Formation (-11.5 to -10.9 ‰, n=3) increase to -8.1 ‰ in the tuffaceous dolomite; the $\delta^{13}C$ values are scattered but generally of higher magnitudes in the cap dolomite (-8.0 to -5.8 ‰, n=5) and the overlying rhythmic deposits (-8.3 to -6.8 ‰, n=6). Overall, the isotopic profile is very variable and exhibits a strong correlation between $\delta^{13}C$ and $\delta^{18}O$ in beds 0-1 (samples 8-11) and 3-7 (samples 16-21), clearly implying that the values of $\delta^{13}C$ in samples 8-11 and 16-21 were affected by diagenesis, whereas those in samples 12-15 of the cap dolomite reflect the original rock formation environment (uncorrelated $\delta^{13}C$ and $\delta^{18}O$ values). However, the $\delta^{13}C$ values in the cap dolomite are more negative (-7.3 to -5.8 ‰, n=4) compared with that in the overlying calcareous mudstone (-6.8 ‰, n=1; Fig.8 and Supplementary Table 1).

4.2.6 Xipocun section at Songluo village (section 6)

In section 6 (Supplementary Fig. 6), the Nantuo Formation (bed 1) consists of grayish–green medium-grained diamictites with clasts of variable sizes (Supplementary Fig. 6-1a). The cap dolomite (Fig. 9, a, bed 2) is 1.8-m thick and consists of grayish–yellow finely crystalline and laminated dolomite (Fig. 9, a and b, bed 2; Supplementary Fig. 6-1 b-f). The bottom region of the cap dolomite contains deformed breccias and the upper part exhibits tepee-like bedding. Microscopically, the cap dolomite is composed of stromatolite-like dolomite, ctenoid-fractured dolomites, and breccias (Fig. 9b). The DST2 unit above the cap dolomite comprises rhythmic deposits consisting of dark gray siltstone and dolomitic mudstone.

The $\delta^{13}C$ values in the Nantuo Formation (-4.6 to -3.0 ‰, n=4), cap dolomite (-4.4 to -2.5 ‰, n=14), and overlying Doushantuo Formation (-4.7 ‰, n=1) are highly variable, displaying a poorly-defined upward increasing trend from the base of the section to the middle part of the cap dolomite member, followed by an upward decreasing trend (Fig. 9 and Supplementary Table 1).

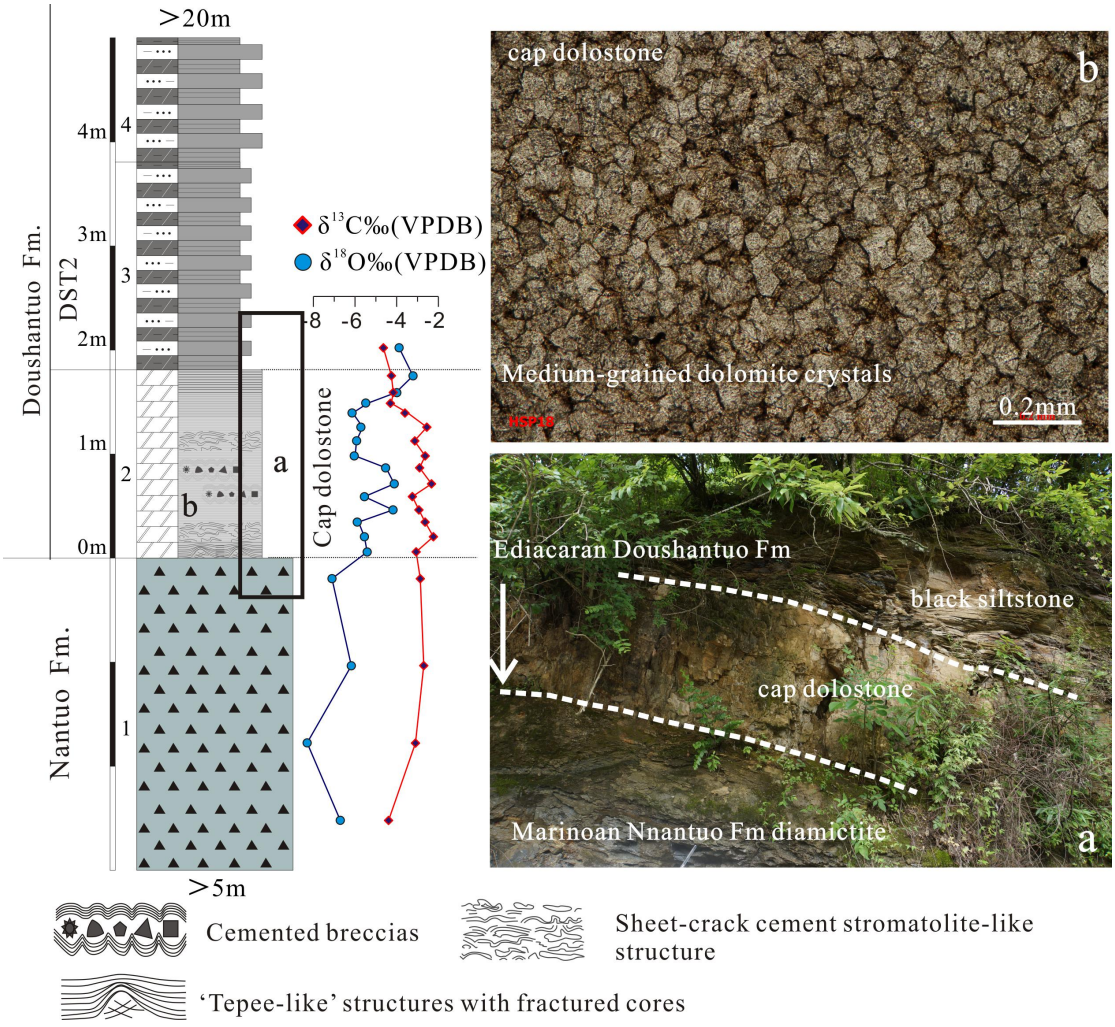

Fig. 9 Chemostratigraphy and sedimentology of the cap dolomite in the Xipocun section (section 6). In the measured section, the numbers indicate beds and the letters marked beside the lithological column indicate the locations of subfigures (a–c). (a) cap dolomite and its contact surfaces with the underlying diamictites of the Nantuo Formation and the overlying siltstone of the Doushantuo Formation; (b) cap dolomites with secondary silicification, and finely crystalline laminated dolomite containing tepee-like structures with fractured cores or stromatolite-like dolomite. $\delta^{18}O$ and $\delta^{13}C$ values shown by the curve are given in Supplementary Table 1. See Fig. 4 for the lithological and sedimentary structures legend. Colors used in the lithological column reflect the surface colors.

5. Interpretations and discussion

5.1 Geochemistry: $\delta^{13}C$ variations in the cap dolomite of Shennongjia

An extreme negative $\delta^{13}C$ deviation is recorded in the sedimentary succession comprising

the diamictites of the Nantuo Formation and the cap dolomite of the Ediacaran Doushantuo Formation in Shennongjia. Most of the Nantuo Formation diamictites display large negative $\delta^{13}C$ deviations (less than -8 ‰) with the extreme negative drift from -11 to -8 ‰ occurred in the Mahuanggou and Guanmenshan sections, whereas the $\delta^{13}C$ values of the cap dolomite fluctuate between -7.3 and -2.5 ‰ (averagely between -5.4 and -4.1 ‰). Above the cap dolomite, $\delta^{13}C$ values display an oscillation with variations between -8 and -4 ‰ (Fig. 10). Bed 3 of the Gaoqiaohe section (Fig. 4) features a microcrystalline fabric, with the occurrences of pyrite and minor siliciclastic components, which are typical characteristics of the cap dolomite (Shields, 2005). In contrast, in the overlying DST2 unit, the presence of dolomite and a greater abundance of siliciclastic components suggest that beds 4-24 do not represent the continuation of the cap dolomite in the Gaoqiaohe section (Fig. 4). The partial yellowish–brown hue is attributed to iron and manganese staining. The rhythmic evolution of lithological changes and $\delta^{13}C$ profile characteristics within these carbonate rocks suggests several explanations. For example, the rhythmicity could be attributed to rapid sea-level oscillations during a post-Marinoan marine transgression. Further, this may also indicate seasonal changes in carbonate production or sediment supply.

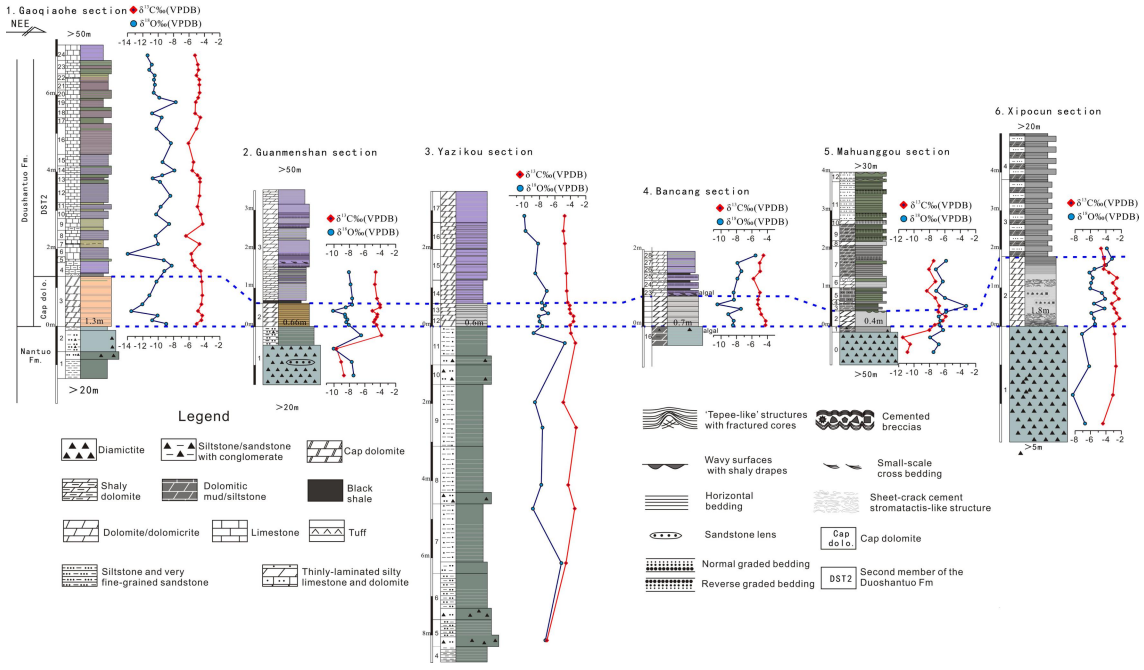

Fig. 10 Correlations of carbon and oxygen isotopes in the Ediacaran cap dolomite of Shennongjia,

in the northern margin of the Yangtze Craton. In the measured section, the numbers indicate beds and the values shown by the curves are given in Supplementary Table 1. The colors used in the lithological column reflect the surface colors.

Globally, Ediacaran cap dolomites display a remarkable $\delta^{13}C$ negative drift, which could suggest a global $\delta^{13}C$ negative drift event. The Ediacaran cap dolomites preserved in North America (James et al., 2001; Corsetti and Grotzinger, 2005; Creveling et al., 2016), India (Jiang et al., 2002), Oman (Allen et al., 2004), Australia (Mazumdar and Kennedy, 1996; Rose and Maloof, 2010), Namibia (Hoffman et al., 2007; Hoffman and Macdonald, 2010), and Central Africa (Mickala et al., 2014) generally show that $\delta^{13}C$ profiles become increasingly negative from the bottom part to the upper part of the cap dolomites with a few exceptions (Fig. 11). For example, the $\delta^{13}C$ profile in North America displays a gentle negative excursion upward and oscillates around -3 ‰ (James et al., 2001; Corsetti and Grotzinger, 2005; Creveling et al., 2016). The $\delta^{13}C$ values in the profile in Ghana display an oscillation around -3 ‰, with a more negative excursion of -7 ‰ upward (Mickala et al., 2014). In Australia, two remarkable negative excursions occur in the lower cap dolomite and are followed by a more negative excursion of -5 ‰ (Mazumdar and Kennedy, 1996; Rose and Maloof, 2010; Liu et al., 2013). In Namibia, a negative oscillation around -2 ‰ is observed in the lower part of the cap dolomite while greater deviations are present in the upper part (Hoffman et al., 2007; Hoffman and Macdonald, 2010).

Further, the $\delta^{13}C$ variation trends, being similar to those worldwide, were observed in South China as well. Although the cap dolomites in Shennongjia are much thinner, and mainly composed of muddy dolomite without typical sedimentary structures, which are common in the cap dolomites in South China (Supplementary Table 2), they all overlie the diamictite of Nantuo Formation (Marinoan Glaciation) and show negative $\delta^{13}C$ values. In Three Gorges area, $\delta^{13}C$ values, mainly ranging from -8 to 0 ‰, is lower than those in Shennongjia area, ranging from -7 to -2 ‰ (Fig. 11). This $\delta^{13}C$ value difference mentioned above probably resulted from the variation of the depositional environment for the cap dolomite precipitation. Compared with the shelf margin area with slightly deeper water, where the Three Gorges area

582 located, Shennongjia was located in the intertidal area with shallower water during the early
583 Ediacaran (Kuang et al., 2019). $\delta^{13}C$ values responding to water depth were reported by Wang
584 et al. (2017) as well. A study on four Ediacaran cap dolomite sections in the Shennongjia area
585 was firstly reported (Wang et al., 2017), but it focused primarily on carbon and oxygen
586 isotope compositions. However, this study provides an integrated study of not only the carbon
587 and oxygen isotope compositions but also sedimentological and lithological analyses, as well
588 as stratigraphic and geochemical correlations of the cap dolomites across the YC. Of the six
589 sections examined in the Shennongjia area in this study, three have been studied by Wang et
590 al. (2017). The results of Wang et al. (2017) differ slightly from the results of the present
591 study, both in terms of compositions and spatial variations of $\delta^{13}C$, which indicate a higher
592 basal $\delta^{13}C$ value and three-times greater oscillation amplitude from lower negative to lower
593 positive $\delta^{13}C$ excursions upward in the Longxi section. Furthermore, Wang et al. (2017)
594 primarily attributed the spatial variation in C-isotopic chemostratigraphy of the cap dolomite
595 in Shennongjia to Marinoan post-glacial sea-level fluctuations. For example, in the Longxi
596 section, early regression (beneath the tepee-like structures) led to intense photosynthesis and a
597 positive $\delta^{13}C$ shift. Late regression (tepee-horizon), then, resulted in a negative $\delta^{13}C$ shift due
598 to sulfate reduction and the influx of freshwater with ^{13}C-depleted dissolved inorganic carbon
599 (DIC), and the following early transgression (uppermost part of the cap dolomite) may reflect
600 stimulated primary productivity, which brought about a positive $\delta^{13}C$ drift.

601 In fact, except for the sea levels changes, numerous hypotheses had been proposed for the
602 C-negative shift of cap dolomite in Precambrian, and these alternative interpretations are
603 worthy of discussion. We believe that:

604 1) The carbon isotopes of the Ediacaran cap dolomite can be correlated between Shennongjia
605 and the other areas worldwide (Jiang et al., 2003a, 2007; Zhu et al., 2007; Yu et al., 2020). They
606 are all negative without exceptions, but the amplitude (absolute value) of C-negative shifts
607 worldwide are not consistent, and there is no fixed range of the negative drift value at all (Fig. 11).

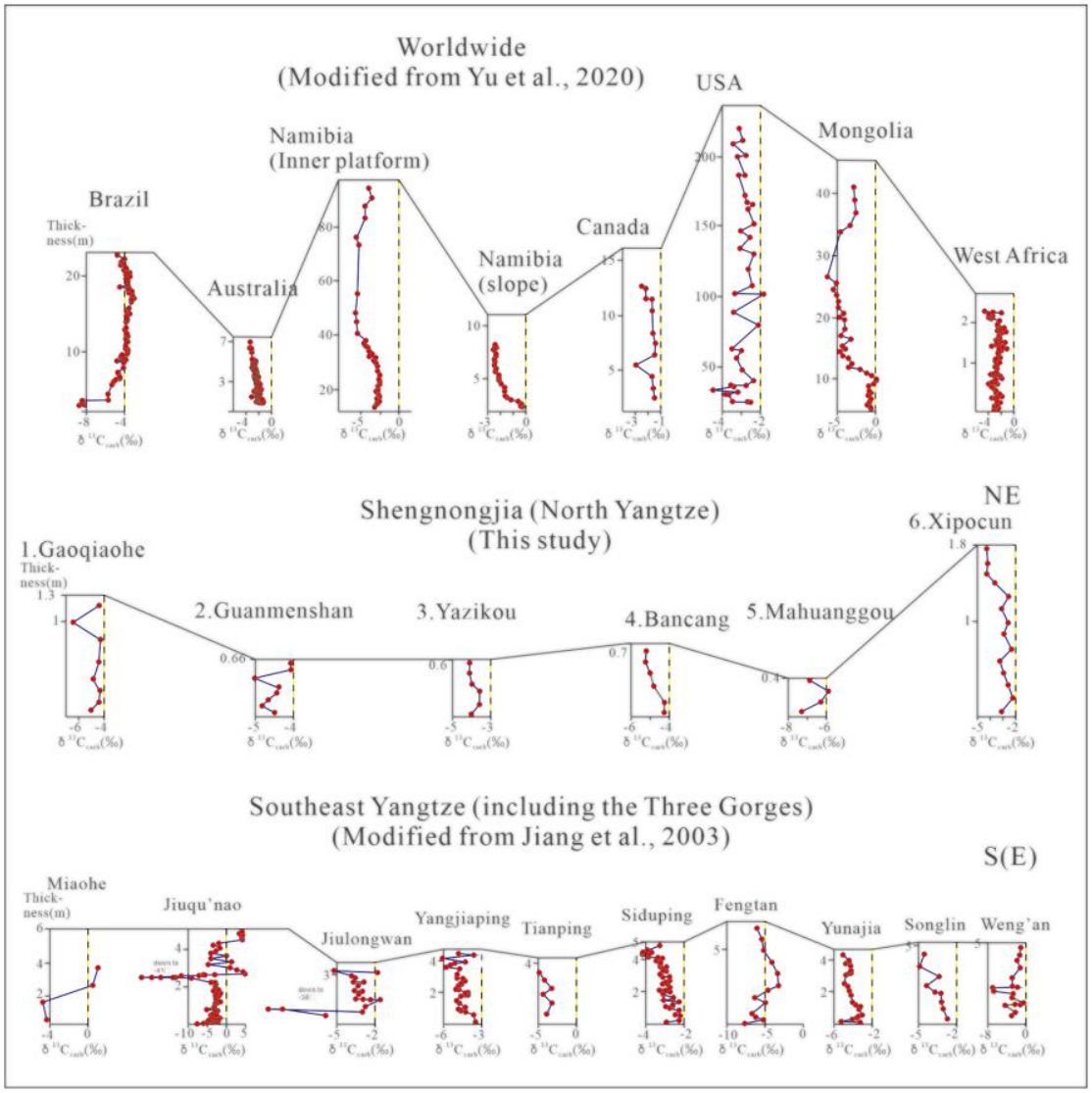

608

609 **Fig. 11 Schematic correlations of the carbon isotopes of the Ediacaran cap dolomites**
610 **worldwide**

611 2) There is no fixed pattern of C-negative drift in the cap dolomite upward, that is, it can be
612 either much more negative upward (great negative) or gradually negative (slightly negative), and it
613 can even be curved with a turning point in the upper or middle part of the cap dolomites.

614 3) There is no consistent rule to follow in C-negative drift pattern or amplitude of the cap
615 dolomite in "relative deep or shallow water" environments. For the C-negative drift of the cap
616 dolomite formed in "shelf and slope" in Namibia, except for the amplitude differences, $\delta^{13}C$ of the
617 shallow water "shelf" deposits shows a more negative drift than that in "deep water slope"
618 deposits. Does this mean that $\delta^{13}C$ should be more negative in shallow water than in "deep water"?
619 Our current study tends to suggest that cap dolomites are all formed in shallow water, and it is true

620 that the $\delta^{13}C$ values of the cap dolomite formed in shallow water are more negative than those
621 formed in “deep water”. However, in the transition area from shallow water to “deep water”,
622 where is adjacent to the edge of rimmed platform, there may be typical cap dolomites resulted
623 from facies variation. In this area, barite fans with high manganese content are well developed,
624 whose formation are interpreted to be related to relative deep water or submarine volcanism and
625 upwelling current (Peng et al., 2011; Lang et al. 2016; Crockford et al., 2019). On the contrary,
626 in the typical deep water environment, we have not seen the typical cap dolomites (such as in
627 Liuchapo, central Hunan Province, and the southeast margin of the Yangtze Craton). Instead, there
628 are dolomites with high manganese content and the rhythmites composed of argillaceous and silty
629 dolomite, and even cherty or siliceous dolomite. We believe that the sea level changes after the
630 end of the Marinoan glaciation is comparable internationally, but the true trigger mechanism and
631 relationship between sea level changes and C isotope shift is yet in debate.
632 4) For the curved carbon isotope pattern, the inflection point appears in the upper or middle part
633 in many cap dolomites. We wonder whether it (inflection point) is possibly related to
634 upwelling-current (barite fan) (Peng et al., 2011; Lang et al. 2016; Crockford et al., 2019) or
635 oxidation event caused by exposure (karst) (Shields, 2005； Zhou et al., 2010; Zhao et al. 2018)?
636 Because barite fans are mostly developed in the upper or middle part of the cap dolomites. We
637 don’t consider the carbon isotope negative shift can resulted from the reoxidation of DOC in deep
638 waters because we discussed and proofed the cap dolomite should form in the shallow water
639 (Shields, 2005; Zhou et al., 2010; Zhao et al. 2018; Yu et al., 2020).
640 5) The $\delta^{13}C$ negative drift of cap dolomites in different parts of the same basin seems to be
641 different, and the high amplitude of $\delta^{13}C$ negative drift occurred more likely in relatively high
642 places with shallow water. For example, in Shennongjia, which was located in the shallow inner
643 ramp, the cap dolomites are thin and have more pebbles and terrigenous clasts inside, implying an
644 affection of the great chemical weathering (Huang et al. 2016) and intense terrigenous supply on
645 the high amplitude of $\delta^{13}C$ negative drift in shallow area.
646 6) Wang et al. (2017) suggest that C-negative shift of cap dolomite in Shennongjia was
647 probably associated with methanogenesis and primary productivity in deep waters. However, we
648 have no evidence about methanogenesis and possible relationship with C-negative shift of cap

649 dolomitein Shennongjia. C-negative shift induced from primary productivity is consistency with
650 the occurrence of a lot of algae in cap dolomite. These algae can even be found in the upper part of
651 the Nantuo Formation in Shennongjia, meaning that before the cap dolomite, ecological recovery
652 were already on going resulted from the repetitive ice melting (Bai et al., 2020; Hu et al., 2020;
653 Chen et al., 2021), and resulted in the high productivity.

654 Finally, the discussion whether the strong $\delta^{13}C$ -negative drift in the upper part of the cap
655 dolomite is due to the continuous ice-melting, which resulted in the injection of a large amount of
656 continental margin fresh water into the basin, or to the shallower depositional environment, which
657 could accept large-scale chemical weathering input from the continent and lead to the $\delta^{13}C$
658 negative shift (Lang et al., 2016), is hindered limited by the current research evidence.

659 5.2 Sedimentary environment and paleogeography of the cap dolomites

660 A variety of models have been proposed for the formation of the cap dolomite. For example,
661 Grotzinger and Knoll (1995) proposed that physical stratification produced a strong
662 surface-to-deep carbon isotope gradient, resulting in surface waters becoming enriched in
663 $\delta^{13}C$, while deeper waters became enriched in $\delta^{12}C$. The cap dolomite is suggested to have
664 formed as high-alkalinity anoxic deep waters upwelled upon deglaciation, mixing with oxic
665 ocean-surface water. Shields (2005) argued that a buoyant surface plume in low-latitude
666 regions spread rapidly to higher latitudes over dense and saline seawater and could be
667 sustained for a long period until vertical mixing occurred. In this scenario, the cap dolomite
668 rapidly formed within the low-salinity plume in the shallow marine environment. Moreover,
669 Hoffman et al (1998) contended that the cap dolomite was formed in the aftermath of the total
670 ice sheet meltdown. In addition, several other interpretations have attributed the formation of
671 the cap dolomite to methane oxidation in a supersaturated ocean following a time of extreme
672 cold. Although these models all incorporate certain geological elements, most of them have a
673 geochemical origin. For the majority of these models, systematic sedimentary proof is lacking
674 and further investigation is required, especially in regards to the formation environment of the
675 cap dolomite in deep or shallow water, which is still debated.

676 In the past two decades, the cap dolomites have been interpreted as deposits originating

677 from a shallow-water shelf, slope, and basin environment. Accordingly, a sedimentary model
678 of deposition ranging from shallow-water shelf to slope and basin has long been accepted
679 worldwide for the formation of cap dolomite (Jiang et al., 2003b, 2006a; Hoffman et al., 2007;
680 2011; Hoffman and Macdonald, 2010; Wang et al., 2014; Creveling et al., 2016). In particular,
681 previous studies (e.g., Hoffman et al., 2011) have indicated that, except for the variation in
682 thickness ranging from a few meters to hundreds of meters, cap dolomites worldwide show
683 similar distinctive sedimentary structures, such as low-angle cross-bedding, giant wave
684 ripples, and sheet-crack cements. Cap dolomites also show similar diagnostic components, i.e.,
685 tepee breccias and tubestone stromatolites, which are considered to be partly formed in deep
686 water and record changes in petrology, sedimentology, biology, mineralogy, and
687 geochemistry after abrupt global warming, which liberated the Earth from global glaciation.
688 However, these particular sedimentary structures are very rare in Shennongjia, where the cap
689 dolomites are very thin and only show very simple and monotonous sedimentary structures,
690 such as laminations or a lack of bedding (Supplementary Table 2). Collectively, this evidence,
691 therefore, points to the deposition of the Shennongjia cap dolomite in restricted low-energy
692 and shallow-water conditions, e.g., shallow-water tidal environments.

693 As previously mentioned, the cap dolomites in Shennongjia exhibit a much smaller
694 thickness, with an average of less than 1.8 m, and display a smaller variation in thickness.
695 However, the thickness of the cap dolomite in the YC is typically 3-4 m and occasionally as
696 large as 10 m in some locations. It is noteworthy that regardless of the thickness of the cap
697 dolomite and its variation in Shennongjia and YC, there is no sign of deep-water deposition.
698 However, the small thickness and limited variation in thickness of the cap dolomite in
699 Shennongjia and the YC require further study. Correlations of thickness and sedimentary
700 features of the cap dolomite in Shennongjia with those in areas 200 km away show that the
701 cap dolomite eventually becomes thicker toward the southeast (Fig. 12 and 13). For example,
702 the homogeneous silty dolomite in the west of Shennongjia is extremely thin (40 cm) with a
703 weak stratification and lack of any other sedimentary structures. However, the thickness of
704 the cap dolomite in Longxi reaches 2.4 m and that in Gaolan is significantly thicker, at 4.5 m,

while the thickness in Jiulongwan is reduced to 3.5 m.

In addition, three vertical units with unique sedimentary textures and structures can be recognized in the spatial and temporal distribution of the cap dolomite. The lower unit consists of heavily silicified dolomite with pebble dolomite, silicified calcareous crusts, breccias, crystal caves, sheet-crack cements, and teepee structures. The middle units are characterized by the presence of teepee structures and low-angle inclined bedding, with multilayer barite fans, as well as cone, column, dome, and laminated stromatolites occurring upward. In the top unit, more abundant barite fans occur, and are overlapped by fine siliceous rocks or shale indicating deep water. Barite fans indicate the redox interface between the shallow subtidal zone and intertidal environment and, therefore, represent the combined result of upwelling and terrigenous supply on the redox surface. In addition, stromatolites with varied morphologies (columnar, wave, and dome) are frequently present in the middle cap dolomite unit and are interpreted as the product of photosynthesis in a shallow-water environment. However, we note that the lower and middle units of the cap dolomite occur only in the east of Shennongjia and the adjacent Three Gorges area, while the upper unit, that is, those homogeneous dolomites with extremely thin thickness and simple composition and structure, is present in the central and western Shennongjia, implying that these were formed by further sea-level rise and carbonate deposition on a shallow-water shelf.

Furthermore, the dynamic formation mechanism of the sedimentary structures of the cap dolomite, reported to originate from deep-water deposition in previous studies (Hoffman et al., 1998; Hoffman and Schrag, 2002; Jiang et al., 2011), is open to further discussion. Carbonate tidal flats may experience water-escape and liquification in response to the release of pore fluid pressure (Corkeron, 2007) or gas expansion (Kennedy et al., 2008). These processes explain how the tepees structures, silicified calcareous crusts, breccias, sheet-crack cements, and silicification formed in the cap dolomite. All these features represent important evidence indicating evaporative tidal flats and very shallow water environments. In addition, the basal part of the cap dolomite is characterized by localized bedding disruption, brecciation, and strongly silicified cementation, which are widespread across the YC, as reported in previous

studies (Jiang et al. 2003a, 2006a, 2006b, 2011). It is believed that these features formed from methane gas and fluids via gas hydrate destabilization (Jiang et al., 2003a, 2006a, 2006b; Wang et al., 2008). A recent interpretation has ascribed these features to karstification immediately following the cap dolomite precipitation, in response to deglacial isostatic rebound (Zhu et al., 2007a; Zhou et al., 2010). Current research suggests that these features represent a combination of soft sediment deformation, dolomitization, silicification, and karstification, involving meteoric water in a very shallow environment.

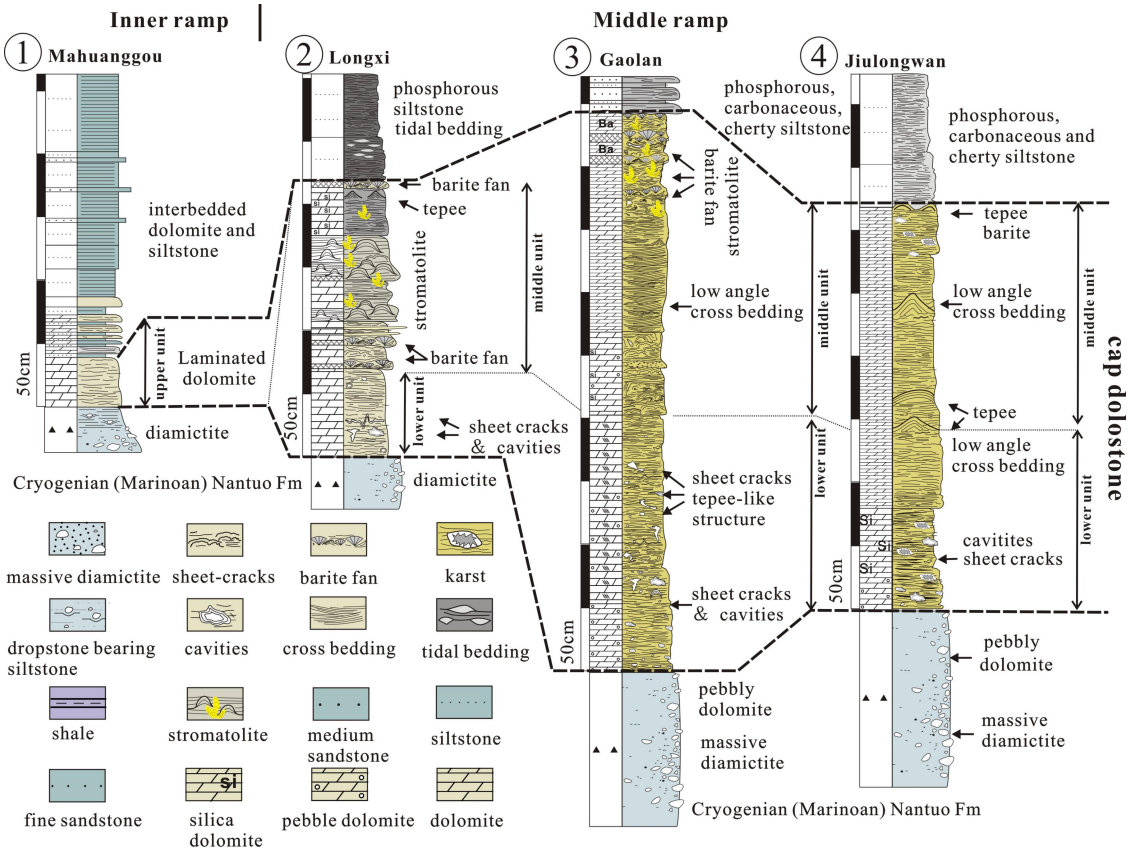

740

741 **Fig. 12 Correlations of the sedimentary facies of the cap dolomite of the Ediacaran Doushantuo**
742 **Formation at Shennongjia with those in nearby areas, and their temporal and spatial**
743 **distribution.**

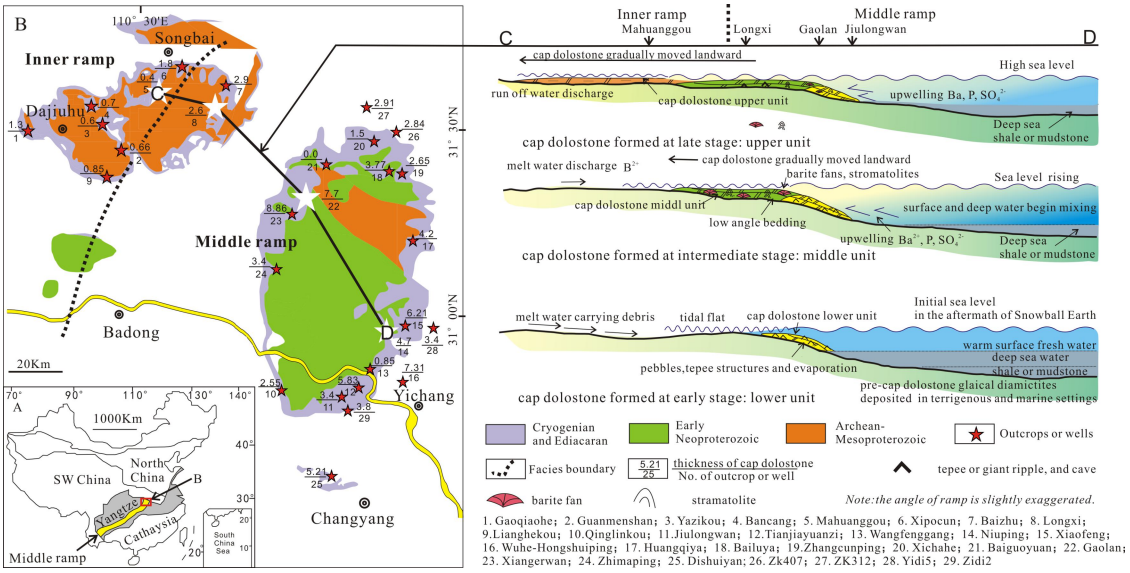

Fig. 13 Proposed model for the formation of the Ediacaran cap dolomite, and sketch of paleogeography for the early Ediacaran Doushantuo Formation in Shennongjia and nearby areas.

In addition, except for the upper unit, the base of the cap dolomite comprising the middle and lower units consists primarily of yellowish-brown dolomites containing gravel. These characteristics are common throughout the YC. The pebbles are rounded-subrounded and their composition is closely associated with the underlying basement rocks, indicating an origin related to local erosion in a shallow-water environment close to the ancient land margin. Moreover, the high calcium content in the cap dolomite and the underlying sediments of the terminal Cryogenian is an indicator of shallow water and a more arid environment. The sedimentary facies formed on the shelf edge (i.e., beach bars and oolitic shoals) and the continental slope are rare in the cap dolomite from Shennongjia to the eastern Three Gorges area; however, tidal facies are spatially and temporally distributed. Such sedimentary facies in the cap dolomite in Shennongjia and nearby areas were deposited on a ramp tilting southeast, influenced by the transgression of the Yangtze Craton Sea.

Finally, we propose a generalized evolution model for the formation of the Ediacaran cap dolomite in terms of deposition on a carbonate ramp in Shennongjia and nearby areas (Fig. 13). The cap dolomite was initially deposited within the lowstand areas landward on a ramp with a slope angle <1° and no shelf break, in response to the first transgression in the

aftermath of snowball Earth (early stage, Fig. 13, lower unit). As a result, more abundant pebbles from the basement rocks were mixed and deposited at the bottom of the cap dolomite during this stage. The sedimentary structures indicating tidal and evaporative environments are very common in the lower unit, such as tepee structures, silicified calcareous crusts, breccias, sheet-crack cements, and silicification (Fig. 14). The following sea-level rise resulted in landward flooding and the deposition of the middle unit of the cap dolomite above the lower unit to catch up with the sea-level rise (middle stage, Fig. 13).

Fig. 14 Sedimentary units within the Ediacaran cap dolomite at Tianjiayuanzi (left) and Jiulongwan (right) in the Three Gorges area.

Due to the frequent upwelling of high-alkalinity anoxic deep waters triggered by transgressive events, repetitive layers of barite rosette aggregates or fans formed on the boundary between the sulfate- and sulfite-seawater, and microbiolites and stromatolites were common in the oxic ocean-surface water in this stage. The transgression did not reach the inner ramp located further landward in the early stage. Therefore, the initial scope of the cap dolomite was limited to the middle ramp, with no effects of upwelling in the initial stage of

sea-level rise, resulting in the rare occurrence of barite. Following the subsequent sea-level rise, the vast transgression reached its maximum landward extent till the inner ramp (shallow-water shelf), where a thin cap dolomite was deposited over the whole shelf. As a result, the new cap dolomite accumulated over the older units, resulting in a thicker cap dolomite. Hoffman et al. (2007) noted that the global average thickness of cap dolomite has been studied stratigraphically in different methods: as a diachronous deposit (top and bottom) tracking glacioeustatic flooding; as a semi-diachronous deposit (bottom diachronous, top isochronous) outlasting the flooding; and as an isochronous deposit (top and bottom) recording ocean-wide changes following deglaciation. Accordingly, our model explains the thickness variations and distribution of cap dolomite at both the local and regional scale. Our model also explains why the cap dolomites in the Shennongjia area share a small thickness and unique sedimentary features, and is interpreted as diachronous deposits (bottom to top). Finally, this model shows that the cap dolomite was originally deposited in shallow water (where all the new cap dolomite formed), but over time, as sea levels rose, the previous shallow area, where cap dolomite formed, became into relatively deep area. At the same time, new cap dolomite is still forming in the new shallow water area. Therefore, the transition of sedimentary environment includes both temporal and spatial changes. In other words, the differences of carbon isotopes in the ramp at Shennongjia area represents both a time dependent record and a spatial carbon isotope gradient. But now, we can't separate a time record from a spatial carbon isotope gradient exactly, including to identify the diachronous cap dolomite in time dependent record clearly.

6. Conclusions

The Ediacaran cap dolomites in the six outcrops studies herein in Shennongjia area, northern Yangtze Craton, South China, are thin, mostly composed of fine crystalline dolomite. Laminae with varying thicknesses developed in the cap dolomite, while the typical sedimentary structures reported worldwide for the cap dolomite are rare or even absent here.

Strong $\delta^{13}C$ variations ranging from -7.3 to -2.5 ‰ are displayed in the cap dolomite in this area. Sedimentological analysis indicates that the cap dolomite was primarily formed in a shallow-water environment. A model of deposition on a ramp is proposed, based on the sedimentological analysis of the early Ediacaran cap dolomites of Shennongjia and the nearby Three Gorges area of the YC. This model explains the thickness variations and the distribution of the cap dolomites at both the local and regional scale, as well as the sedimentary structures, composition, and barite occurrence; it also explains the precipitation of uniquely thin cap dolomite in the Shennongjia area. Finally, the cap dolomite is interpreted as a diachronous deposit (bottom to top), tracking glacioeustatic flooding and recording ocean-wide changes following deglaciation, in accordance with the concept of Hoffman et al. (2007).

Acknowledgements

This research was co-supported by the Peking International Innovation and Resource Cooperation Program “The Precambrian last glaciation and the evolution of paleoenvironment and life on Earth” (Z201100008320007), the National Key Research and Development Program of China (2016YFC0601001), the National Natural Science Foundation of China (42072135, U19B6003 and 41472082), China Geological Survey (DD20190005, DD20190002), Surplus funds “Research on the Neoproterozoic stratigraphic pattern and depositional characteristics in Shennongjia” (AS2101) and the Shennongjia National Geopark. We are grateful to Prof. Yuansheng Geng for his valuable guidance and discussion, and grateful to Prof. Lesheng Qu from Hubei Geological Survey for the careful field direction. Sincere thanks are also given to Mr. Wei Cao from Department of Natural Resources of Hubei Province, Profs. Zejiu Wang, Jianxin Yao, Mr. Xin Shang and Mrs. Xiulan Ma from Chinese Academy of Geological Sciences (CAGS) and China Commission of Stratigraphy. Great thanks to Graduate students Zhengxiu Fan for her contribution on drawing figures. Thanks for three anonymous reviewers and the editor’s active and constructive suggestions and comments.

References

Allen P. A., Leather J., Brasier M. D.,2004. The Neoproterozoic Fiq glaciation and its aftermath, Huqf supergroup of Oman. Basin Research 16: 507—534

An, Z. H., Jiang, Q. G., Tong, J. N., Tian, L., Ye, Q., Song, H., Song, H., 2015. Stratigraphic position of the Ediacaran Miaohe biota and its constrainson the age of the upper Doushantuo $\delta^{13}C$ anomaly in the YangtzeGorges area, South China. Precambrian Research 271, 243–253.

Bai, H. Q., Kuang, H. W., Liu, Y. Q., Peng, N., Chen, X. S., Wang, Y. C., 2020. Marinoan-aged red beds at Shennongjia, South China: Evidence against global-scale glaciation during the Cryogenian. Palaeogeography Palaeoclimatology Palaeoecology 559:109967.

Banner, J. L., Hanson, G. N., 1990. Calculation of simultaneous isotopic and trace element variations during water–rock interaction with applications to carbonate diagenesis. Geochim. Cosmochim. Acta 54, 3123-3137.

Banner, J. L., Kaufman, J., 1994. The isotopic record of ocean chemistry and diagenesis preserved in non-luminescent brachiopods from Mississippian carbonate rocks, Illinois and Missouri. GSA Bull 106, 1074-1082

Bartley, J. K., Kah, L. C., Mcwilliams, J. L., Stagner, A. F., 2007. Carbon isotope chemostratigraphy of the middle riphean type section (avzyan formation, southern urals, russia): signal recovery in a fold-and-thrust belt. Chemical Geology 237(1-2), 211-232.

Chen, X. S., Kuang, H. W., Liu, Y. Q., Le Heron, D. P., Wang, Y. C., Peng, N., Wang, Z. X., Zhong, Q., Yu, H. L., Chen, J. X., 2021. Revisiting the Nantuo Formation in Shennongjia, South China: A new depositional model and multiple glacial cycles in the Cryogenian. Precambrian Research 356:106132.

Christie-Blick, N. Soh, L. E., 1999. Considering a Neoproterozoic snowball earth. Science 284, 1087-1088.

Condon, D., Zhu, M., Bowring, S., Wang, W., Yang, A., Jin, Y., 2005. U-Pb ages from the Neoproterozoic Doushantuo Formation, China. Science 308, 95-98.

Corkeron, M., 2007. “Cap carbonates” and Neoproterozoic glacigenic successions from the Kimberley region, north-west Australia. Sedimentology 54, 871-903. http://doi.org/10.1111/j.1365-3091.2007.00864.x.

Corsetti, F. A., Grotzinger, J. P., 2005. Origin and significance of tube structures in Neoproterozoic post-glacial cap carbonates: example from noonday Dolomite, Death Valley, United States. Palaios 20, 348-362. http://doi.org/10.2307/27670350

Creveling, J.R., Bergmann, K.D., Grotzinger, J.P., 2016. Cap carbonate platform facies model, Noonday Formation, SE California. GSA Bulletin 128, 1249-1269. http://doi.org/10.1130/B31442.1.

Crockford, P. W., Wing, B. A., Paytan, A., Hodgskiss, M. S., Mayfield, K. K., Hayles, J. A., Middleton, J, E., Ahm, A, S, C., Johnston, D, T., Caxito, F., Uhlein, G., Halverson, G, P.,

Eickmann, B., Torres, M., Horner, T. J., 2019. Barium-isotopic constraints on the origin of post-Marinoan barites. Earth and Planetary Science Letters 519, 234-244.

Deng, Q., Shi, X., Du, X., 2015. Stratigraphic Sequence and Sedimentary Characteristics of Nanhua System in Mahuanggou, Shennongjia Area. Resoures Environment & Engineering 29(2), 124-131.

Doe, B. R., 1973. Strontium isotope geology. Earth Science Reviews 9(2), 150-151.

Faure, G. 1977. Principles of isotope Geology. New York: John Wiley Sons, 97-146.

Frank, T.D., Lyons, T.W., 2000. The integrity of δ18O records in Precambrian carbonates: a Mesoproterozoic case study. In: Grotzinger, J.P., James, N.P. (Eds.), Carbonate Sedimentation and Diagenesis in the Evolving Precambrian World. SEPM Special Publication 67, 315-326.

Geng, Y., 2015. Neoproterozoic Era of South China Craton. In: Zhai M. G. (ed.), Precambrian Geology of China. Berlin: Springer-Verlag Berlin Heidelberg 390. http://doi.org/10.1007/978-3-662-47885-1.

Grotzinger, J. P., Knoll, A. H., 1995. Anomalous carbonate precipirates: Is the Precambrian the key to the Permian?.Palaios 10, 578-596.

Guan, K., Tian, L., An, Z., Hu, J., Tong, J., 2016. Stratigraphic succession of the Nanhuan period in the Shennongjia area in western Hubei and its regional correlation. Earth Science Frontiers 3, 236-245(in Chinese with English abstract).

Halverson, G. P., Hoffman, P. F., Schrag, D. P., Maloof, A. C., Rice, A. H. C., 2005. Toward a Neoproterozoic composite carbon-isotope record. GSA Bulletin 117, 1181-1207. https://doi.org/10.1130/B25630.1.

Hoffman, P. F., Halverson, G. P., Domack, E. W., Husson, J. M., Higgins, J. A., Schrag, D. P., 2007. Are basal Ediacaran (635 Ma) post-glacial “cap dolostones” diachronous? Earth and Planetary Science Letter 258, 114-131. http://doi.org/10.1016/j.epsl.2007.03.032.

Hoffman, P. F., Kaufman, A. J., Halverson, G. P. and Schrag, D. P., 1998. A Neoproterozoic Snowball Earth. Science 281, 1342-1346. http://doi.org/10.1126/science.281.5381.1342.

Hoffman, P. F., Schrag, D. P., 2002. The snowball earth hypothesis: testing the limits of global change. Terra Nova 14, 129-155. http://doi.org/10.1046/j.1365-3121.2002.00408.x.

Hoffman, P. F., Macdonald, F. A., 2010. Sheet-crack cements and early regression in Marinoan (635 Ma) cap dolostones: Regional benchmarks of vanishing ice-sheets? Earth and Planetary Science Letters 300, 374-384. http://doi.org/10.1016/j.epsl.2010.10.027.

Hoffman, P. F., Macdonal, D. F. A., Halverson, G. P., 2011. Chemical sediments associated with Neoproterozoic glaciation: Iron formation, cap carbonate, barite and phosphorite. From Aenaud, E., Halverson, G. P. & Shields-Zhou, G. (Eds) The Geological Record of Neoproterozoic Glaciation. Geological Society, London, Memoirs 36, 67-80. http://doi.org/10.1144/M36.5.

Hu, J., Li, C., Tong, J. N., Ye Q., Tian, L., An, Z. H., Dodd, M., Algeo, T. J. 2020. Glacial origin

910 of the Cryogenian Nantuo Formation in eastern Shennongjia area (South China): Implications
911 for macroalgal survival - ScienceDirect. Precambrian Research 351:105969.
912 Huang, K. J., Teng, F. Z., Shen, B., Xiao, S., Lang, X., Ma, H. R., Fu, Y., Peng, Y., 2016. Episode
913 of intense chemical weathering during the termination of the 635Ma Marinoan glaciation.
914 Proceedings of the National Academy of Sciences 113: 14904-14909.
915 James, N. P., Narbonne, G. M., Kyser, T. K., 2001. Late Neoproterozoic cap carbonates:
916 Mackenzie Mountains, northwestern Canada: precipitation and global glacial melt down.
917 Cannada Journal Earth Science 38, 1229-1262. http://doi.org/10.1139/e01-046.
918 Jiang, G., Christie-Blick, N., Kaufman, A.J., Banerjee, D.M., Rai, V., 2002. Sequence stratigraphy
919 of the Neoproterozoic Infra Krol Formation and Krol Group, Lesser Himalaya, India. Journal
920 of Sedimentary Research 72, 524–542.
921 Jiang, G., Kennedy, M. J., Christie-Blick, N., 2003a. Stable isotopic evidence for methane seeps in
922 Neoproterozoic postglacial cap carbonates. Nature 426, 822-826.
923 http://doi.org/10.1038/nature02201.
924 Jiang, G.Q., Sohl, L.E., Christie-Blick, N., 2003b. Neoproterozoic stratigraphic comparison of the
925 Lesser Himalaya (India) and Yangtze block (south China): Paleogeographic implications.
926 Geology 31, 917-920.
927 Jiang, G., Kennedy, M.J., Christie-Blick, N., Wu, H., Zhang, S., 2006a. Stratigraphy, sedimentary
928 structures, and textures of the late neoproterozoic doushantuo cap carbonate in south China.
929 Journal of Sedimentary Research 76, 978-995. https://doi.org/10.2110/jsr.2006.086.
930 Jiang, G., Shi, X., Zhang, S., 2006b. Methane seep structure hydrate decomposition release and
931 late Neoproterozoic ice cap carbonate rocks. Chinese Science Bulletin 51(10):1121-1138
932 Jiang, G., Kaufman, A. J., Christie-Blick, N., Zhang, S., Wu, H., 2007. Carbon isotope variability
933 across the Ediacaran Yangtze platform in South China: Implications for a large
934 surface-to-deep ocean $\delta^{13}C$ gradient. Earth and Planetary Science Letters 261, 303-320.
935 http://doi.org/10.1016/j.epsl.2007.07.009.
936 Jiang, G., Shi, X., Zhang, S., Wang, Y., Xiao, S., 2011. Stratigraphy and paleogeography of the
937 Ediacaran Doushantuo Formation (ca. 635–551 Ma) in South China. Gondwana Research 19,
938 831–849. http://doi.org/10.1016/j.gr.2011.01.006.
939 Kah, L. C., 2000. Depositional $\delta^{18}O$ signatures in Proterozoic dolostones: constraints on seawater
940 chemistry and early diagenesis. In: Grotzinger, J.P., James, N.P. (Eds.), Carbonate
941 Sedimentation and Diagenesis in the Evolving Precambrian World. SEPM Special
942 Publication, SEPM, Tulsa 67, 345-360.
943 Kaufman, A. J., Hayes, J. M., Knoll, A. H., Germs, G.J.B., 1991. Isotopic compositions of
944 carbonates and organic carbon from upper Proterozoic successions in Namibia; stratigraphic
945 variation and the effects of diagenesis and metamorphism. Precambrian Research 49,
946 301-327
947 Kaufman, A. J., Knoll, A. H., Narbonne, G. M., 1997. Isotopes, ice ages, and terminal Proterozoic

948 earth history. Geology 94, 6600-6605. http://doi.org/10.1073/pnas.94.13.6600.
949 Kaufman, A.J., Jacobsen, S.B., Knoll, A.H., 1993. The Vendian record of Sr and C isotopic
950 variations in seawater: implications for tectonics and paleoclimate. Earth Planet. Sci. Lett.
951 120, 409-430
952 Kennedy, M. J., Christie-Blick, N., 2001a. Carbon isotopic composition of Neoproterozoic glacial
953 carbonates as a test of paleoceanographic models for snowball earth phenomena. Geology 29,
954 1135-1138. http://doi.org/10.1130/0091-7613(2001)029<1135:cicong>2.0.co;2.
955 Kennedy, M. J., Christie-Blick, N., 2001b. Are Proterozoic cap carbonates and isotopic excursions
956 a record of gas hydrate destabilization following Earth's coldest intervals?.Geology 29,
957 443-446. http://doi.org/10.1130/0091-7613(2001)029<0443:apccai>2.0.co;2.
958 Kennedy, M. J., Mrofka, D., Von Der Borch, C., 2008. Snowball Earth termination by
959 destabilization of equatorial permafrost methane clathrate. Nature 453, 642-645.
960 http://doi.org/10.1038/nature06961.
961 Kuang, H., Geng, Y., Liu, Y., Wang, Y., Xia, X., Peng, N., Fan, Z., Chen, X., Bai, H., 2019.
962 Revision of "the bottom of Shennongjia Group" and stratigraphic implication in the northern
963 margin of Yangtze Craton. Acta Geologica Sinica 93(1), 72-93(in Chinese with English
964 abstract).
965 Lan, Z., Li, X., Zhang, Q., Li, Q., 2015. Global synchronous initiation of the 2nd episode of
966 Sturtian glaciation: SIMS zircon U-Pb and Oisotope evidence from the Jiangkou Group,
967 South China. Precambrian Research 267, 28-38.
968 https://doi.org/10.1016/j.precamres.2015.06.002.
969 Lang, X., Shen, B., Peng, Y., Huang, K., Lv, J., Ma, H., 2016. Ocean oxidation during the
970 deposition of basal Ediacaran Doushantuo cap carbonates in the Yangtze Platform, South
971 China. Precambrian Research 281, 253-268.
972 Li, Q., Leng, J., 1987. The upper Precambrian in the Shennongjia region. Tianjin: Science and
973 Technology Publishing House 1-503(in Chinese).
974 Liu, C., Wang, Z., Raub, T.D., 2013. Geochemical constraints on the origin of Marinoan cap
975 dolostones from Nuccaleena Formation, South Australia. Chemical Geology 351, 95-104.
976 http://doi.org/10.1016/j.chemgeo.2013.05.012.
977 Liu, C., Wang, Z., Timothy, D.R., Francis, A.M., David, A.D.E., 2014a. Neoproterozoic
978 cap-dolostone deposition in stratified glacial meltwater plume. Earth and Planetary Science
979 Letters 404, 22-32. http://doi.org/10.1016/j.epsl.2014.06.039.
980 Liu, P., Xiao, S., Yin, C., Chen, S., Zhou, C., Li, M., 2014b. Ediacaran acanthomorphic acritarchs
981 and other microfossils from chert nodules of the upper doushantuo formation in the yangtze
982 gorges area, south china. Journal of Paleontology 88, 1-139.
983 Lu, S., Ma, G., Gao, Z., Lin, W., 1985. Sinian ice ages and glacial sedimentary facies-areas in
984 China. Precambrian Research 29, 53-63. http://doi.org/10.1016/0301-9268(85)90059-2.
985 Lu, S., Qu., L., 1987. Characteristics of the Sinian glaciogenic rocks of the Shennongjia region,

Hubei Province, China. Precambrian Research 36, 127-142. http://doi.org/10.1016/0301-9268(87)90085-4.

Mazumdar, A., Kennedy, M. J., 1996. Stratigraphy, sedimentology, and isotopic geochemistry of Australian Neoproterozoic postglacial cap dolostones: deglaciation, $\delta^{13}C$ excursions, and carbonate precipitation. Journal of Sedimentary Research 66, 1050-1064. http://doi.org/10.2110/jsr.66.1050.

Mickala, O. R., Vidal, L., Boudzoumou, F., Affaton, P., Vandamme, D., Borschneck, D., Miche, H., 2014. Geochemical characterization of the Marinoan Cap Carbonate of the Niari-Nyanga Basin, Central Africa. Precambrian Research 255, 367-380. http://doi.org/10.1016/j.precamres.2014.10.001.

Peng, Y., Bao, H., Zhou, C., Yuan, X., 2011. ^{17}O-depleted barite from two Marinoan cap dolostone sections, South China. Earth and Planetary Science Letters 305, 21-31.

Peng, Y., Peng, Y., Lang, X., Ma, H., Huang, K., Li, F., Shen, B., 2016. Marine Carbon-Sulfur Biogeochemical Cycles during the Steptoean Positive Carbon Isotope Excursion (SPICE) in the Jiangnan Basin, South China. Journal of Earth Science 26(2), 242-254.

Porter, S.M., Knoll, A.H., Affaton, P., 2004. Chemostratigraphy of Neoproterozoic cap carbonates from the Volta basin, West Africa. Precambrian. Research 130, 99-112. http://doi.org/10.1016/j.precamres.2003.10.015.

Ridgwell, A. J., Kennedy, M. J., Caldeira, K., 2003. Carbonate deposition, climate stability, and Neoproterozoic ice ages. Science 302, 859-862. 10.1126/science.1088342

Rose, C. V., Maloof, A. C., 2010. Testing models for post-glacial cap dolostone deposition: Nuccaleena Formation, South Australia. Earth and Planetary Science Letters 296, 165-180. http://doi.org/10.1016/j.epsl.2010.03.031.

Schobben, M., Ullmann, C.V., Leda, L., Korn, D., Struck, U., Reimold, W. U., Ghaderi, A., Algeo, T. J., Korte, C., 2016. Discerning primary versus diagenetic signals in carbonate carbon and oxygen isotope records: An example from the Permian-Triassic boundary of Iran. Chemical Geology 422, 94-107. http://doi.org/10.1016/j.chemgeo.2015.12.013.

Shen, Y., Zhang, T., Chu, X., 2005. C-isotopic Stratification in a Neoproterozoic Postglacial Ocean. Precambrian Research 137(3-4), 243–251. http://doi:10.1016/j.precamres.2005.03.004

Shields, G. A., 2005. Neoproterozoic cap carbonates: a critical appraisal of existing models and the plume world hypothesis. Terra Nova 17, 299-310. http://doi.org/10.1111/j.1365-3121.2005.00638.x.

Shu, L., Faure, M., Yu, J., Jahn, B. M., 2011. Geochronological and geochemical features of the Cathaysia block, South China: new evidence for the Neoproterozoic breakup of Rodinia. Precambrian Research 187, 263-276. http://doi.org/10.1016/j.precamres.2011.03.003.

Song, G., Wang, X., Shi, X., Jiang, G., 2017. New U-Pb age constraints on the upper Banxi Group and synchrony of the Sturtian glaciation in South China. Geoscience Frontiers 8(5),

1161-1173. http://doi.org/10.1016/j.gsf. 2016.11.012.

Veizer, J., Hinton, R. W., Clayton, R. N., & Lerman, A., 1987. Chemical diagenesis of carbonates in thin-sections: Ion microprobe as a trace element tool. Chemical Geology 64(3-4), 225-237. doi:10.1016/0009-2541(87)90004-0.

Walter, M. R., Veevers, J. J., Calver, C. R., Gorjan, P., Hill, A. C., 2003. Dating the 840-544Ma Neoproterozoic interval by isotopes of Strontium, carbon, and sulfur in seawater, and some interpretative models. Precambrian Research 100, 371-433. http://doi.org/10.1016/S0301-9268(99)00082-0.

Wang, G., Wang, J., Wan, Z., Chen, C., Yan, J., 2017. Carbon isotope gradient of the Ediacaran cap carbonate in the Shennongjia Area and its implications for ocean stratification and palaeogeography. Journal of Earth Science 28, 187-195. http://doi.org/10.1007/s12583-016-0923-x.

Wang J. S., Jiang G. Q., Xiao S. H., Li Q., Qing W., 2008. Carbon isotope evidence for widespread methane seeps in the ca. 635 Ma Doushantuo cap carbonate in south China, Geology 36(5), 347-350.

Wang, Z., Jiang, H., Wang, T., Gu, Z., Huang, S., 2014. Hydrocarbon systems andexploration potentials of Neoproterozoic in the Upper Yangtze region. Natural Gas Industry 34, 27-36 (in Chinese with English abstract).

Wang, Z., Wang, J., Du, Q., Deng, Q., Yang, F., 2013. Mature Archean continental crust in the Yangtze Craton: Evidence from petrology, geochronology and geochemistry. Chinese Science Bulletin 58, 2360-2369. http://doi.org/10.1007/s11434-013-5668-7.

Xiao, S., Bao, H., Wang, H., Kaufman, A.J., Zhou, C., Li, G., Yuan, X., Ling, H., 2004. The Neoproterozoic Quruqtagh Group in eastern Chinese Tianshan: evidence for a post-Marinoan glaciation. Precambrian Research 130, 1-26. http://doi.org/10.1016/j.precamres.2003.10.013.

Xiao, S., Muscente, A. D., Chen, L., Zhou, C., Schiffbauer, J. D., Wood, A. D., Polys, N. F., Yuan, X., 2014. The Weng'an biota and the Ediacaran radiation of multicellular eukaryotes. Nat Sci Rev 1, 498-520.

Yang, X., Long, X., Li, J., Dong, Y., Zhao, B., 2019a. Mo isotopic response to the end of Neoproterozoic Marinoan Glaciation: Evidence from a sedimentary profile in South China, Precambrian Research. https://doi.org/10.1016/j.precamres.2020.105609.

Yang, F., Zhou, X., Peng, Y., Song, B., Kou, X., 2019b. Evolution of Neoproterozoic basins within the Yangtze Craton and its significance for oil and gas exploration in South China: An overview. Precambrian Research 337, 1-20. http://doi.org/10.1016/j.precamres.2019.105563.

Yao, J., Shu, L., Santosh, M., Li, J., 2015. Neoproterozoic arc-related andesite and orogeny-related unconformity in the eastern Jiangnan orogenic belt: constraints on the assembly of the Yangtze and Cathaysia blocks in South China. Precambrian Research 262, 84-100. http://doi.org/10.1016/j.precamres.2015.02.021.

Yao, J., Shu, L., Cawood, P.A., Li, J., 2016. Delineating and characterizing the boundary of the

Cathaysia Block and the Jiangnan orogenic belt in South China. Precambrian Research 275, 265-277. http://doi.org/10.1016/j.precamres. 2016.01.023.

Ye, Q., Tong, J., Xiao, S., Zhu, S., An, Z., Tian, L., Hu, J., 2015. The survival of benthic macroscopic phototrophs on a Neoproterozoic snowball Earth. Geology 43, 507-510.

Yin, C., Liu, P., Chen, S., Tang, F., Gao, L., Wang, Z., 2009a. Acriarch biostratigraphic succession of the Ediacaran Doushantuo Formation in the Yangtze Gorges. Acta Palaeontologica Sinica 48, 146-154 (in Chinese with English abstract).

Yin, C., Tang, F., Liu, P., Gao, L., Wang, Z., Chen, S., 2009b. New Advances in the Study of Biostratigraphy of the Sinian (Ediacaran) Doushantuo Formation in South China. Acta Geologica Sinica-English Edition 30, 421-432(in Chinese with English abstract).

Yin, C.Y., Gao, L.Z., 2013. Definition, time limit and stratigraphic subdivision of the Nanhuan System in China. Journal of Stratigraphy 37, 534e541 (in Chinese with English abstract).

Yin, L., Zhu, M., Knoll, A. H., Yuan, X., Zhang, J., Hu, J., 2007. Doushantuo embryos preserved inside diapause egg cysts. Nature 446, 661-663.

Yu, W. C., Algeo T. J., Zhou Q., Du Y. S., Wang, P., 2020. Cryogenian cap carbonate models: a review and critical assessment. Palaeogeography Palaeoclimatology Palaeoecology 552:109727.

Zhang, G., Guo, A., Wang, Y., Li, S, Dong, Y., Liu, S., He, D., Cheng, S., Lu, R., Yao, A., 2013a. Tectonics of South China Continent and its implications. Science China: Earth Sciences 56, 1804-1828. http://doi.org/10.1007/s11430-013-4679-1.

Zhang, Y., Wang, Y., Geng, H., Zhang, Y., Fan, W., Zhong, H., 2013b. Early Neoproterozoic, (850 Ma) back-arc basin in the Central Jiangnan Orogen (Eastern South China): geochronological and petrogenetic constraints from meta-basalts. Precambrian Research 231, 325-342. http://doi.org/10.1016/j.precamres.2013.03.016.

Zhang, H., Hu, Z., Yan, D., Li, C., 2013c. Phosphoric rock series in the Ediacaran Doushantuo age (Sinian period) in western Hubei. Journal of Stratigraphy 37(4), 521-526.

Zhang, Q., Chu, X., 2007. Problems in defining the Nanhua Period. Journal of stratigraphy 31, 222-228 (in Chinese with English abstract).

Zhao, G., Cawood, P.A., 2012. Precambrian geology of China. Precambrian Research 222-223, 13-54

Zhao, G., 2015. Jiangnan Orogen in South China: Developing from divergent double subduction. Gondwana Research 27, 1173-1180. http://doi.org/10.1016/j.gr.2014.09.004.

Zhao, Y. Y., Zhao, M. Y., Li, S. Z., 2018. Evidences of hydrothermal fluids recorded in microfacies of the ediacaran cap dolostone: geochemical implications in south china. Precambrian Research 306.

Zhou, C., Tucker, R., Xiao, S., Peng, Z., Yuan, X., Chen, Z., 2004. New constraints on the ages of Neoproterozoic glaciations in south China. Geology 32, 437-440. http://doi.org/10.1130/g20286.1.

Zhou, C., Bao, H., Peng, Y., Yuan, X., 2010. Timing the deposition of ^{17}O-depleted barite at the aftermath of Nantuo glacial meltdown in South China. Geology 38, 903-906. http://doi.org/10.1130/G31224.1.

Zhou, C., 2016. Neoproterozoic lithostratigraphy and correlation across the Yangtze Block, South China. Journal of Stratigraphy 40, 120-135 (in Chinese with English abstract).

Zhou, C., Yuan, X., Xiao, S., Chen, Z., Hua, H., 2019a. Ediacaran integrative stratigraphy and timescale of China. Science China Earth Sciences 62, 7-24.

Zhou, C., Huyskens, M.H., Lang, X.G., Xiao, S.H., Yin, Q.Z., 2019b. Calibrating the terminations of Cryogenian global glaciations. Geology 1,1–4. https:// doi .org /10 .1130 /G45719.1

Zhu, M., Strauss, H., Shields, G. A., 2007a. From Snowball Earth to the Cambrian bioradiation: calibration of Ediacaran-Cambrian Earth history in South China. Palaeogeography Palaeoclimatology Palaeoecology 254, 1-6. http://doi.org/10.1016/j.palaeo.2007.03.026.

Zhu, M., Zhang, J., Yang, A., 2007b. Integrated Ediacaran (Sinian) chronostratigraphy of South China. Palaeogeography Palaeoclimatology Palaeoecology 254, 7-61. http://doi.org/10.1016/j.palaeo.2007.03.025.

Zhu, M., Lu, M., Zhang, J., Zhao, F., Li, G., Yang, A., Zhao, X., Zhao, M., 2013. Carbon isotope chemostratigraphy and sedimentary facies evolution of the Ediacaran Doushantuo Formation in western Hubei, South China. Precambrian Research 225, 7-28. http://doi.org/10.1016/j.precamres.2011.07.019.

Zhu, M., Yang, J., Yang, A., Li G., Zhao, F., Lv, M., Ying, Z., 2016. Development and sedimentary environment of Neoproterozoic strata, source-reservoir-cap rocks in Southern China. In: Su S. and Wang T. (Eds), 2016. Meso-Neoproterozoic geology and oil and gas resources in eastern China. Beijing: Science Press, 1-565.